FUEL FRAGMENTATION BY FISSION GASES
DURING RAPID HEATING

D. H. Worledge

Sandia National Laboratories

SF 2900-Q(3-80)

8008120277

NOTICE

FUEL FRAGMENTATION BY FISSION GASES DURING RAPID HEATING

D. H. Worledge[†]

Sandia Laboratories, Albuquerque, NM 87185

Abstract

Criteria for the advance of cracks between fission
gas bubbles have been developed for application to LMFBR
irradiated fuel under transient heating conditions. The
criteria involve stress states, differential and total
energy conditions, and mass transfer at the crack. Three
experiments have been analyzed using a model of gas behav-
ior which treats both intragranular and intergranular gas
bubbles as mobile, non-equilibrium entities. In one
experiment which showed fine-scale fuel dispersal in the
solid state, these postulated dispersal criteria were cal-
culated to be satisfied. Calculations were performed for
a number of hypothetical transients. The trend of the
results indicates that heating at 100 K/ms produces the
grain boundary cracking conditions rather easily, a few
hundred degrees below the melting point. Heating rates
of 1 K/ms do not in general lead to the cracking condi-
tions.

Acknowledgments

2

Contents

Illustrations

Tables

4

FUEL FRAGMENTATION BY FISSION GASES DURING RAPID HEATING

D. H. Worledge

1. INTRODUCTION

In postulated LMFBR accidents affecting the integrity of the fuel pins the mode by which mechanical stability is lost is capable of influencing subsequent developments. Such modes include slumping, swelling, fine-scale disintegration, and various modes of entrainment in ambient fluid streams. Moreover, under prompt burst conditions the work potential of expanding fuel vapor is a sensitive function[1,2] of the ability of fission product gases to cause fuel dispersal milliseconds before dispersal would occur from fuel vapor alone. The first stage in fuel dispersal under these conditions may be caused by fine-scale fracturing due to stresses from fission gas bubbles. In several out-of-pile experiments[3] and in two in-pile[4] experiments fuel disruption has been visually recorded, and although for the in-pile experiments the scale of fragmentation has not been closely investigated, the visual record is consistent with breakup on a scale of grain s~~~~~ (~ 0.01 mm). The out-of-pile experiments, performed at Argonne National Laboratory, consist of a series of transients using direct electrically heated (DEH) pins intended to reproduce fuel behavior under conditions typical of a loss-of-flow accident in an LMFBR. In most of these experiments the fuel was heated to around the melting temperature over about 10 seconds although some were run over times as short as 2 seconds and others for as long as 20 seconds.

Maximum heating rates were of the order of 2 K/ms near the end of the transients. Fuel disruption was generally associated with fuel melting and no fine-scale fragmentation was clearly observed as a major disruption mode. The in-pile experiments[4] referred to consist of a series of multipulse Fuel Disruption (FD1) experiments in the ACPR reactor at Sandia Laboratories. The fuel was fission heated, and two experiments with the highest heating rates ($\sim$ 100 K/msec) exhibited fine-scale disruption close to but distinctly below the melting point.[5] Some other experiments in the FD1 series having slower heating rates exhibited rapid gross swelling[4] ($\sim$ 60 volume %). These experiments had maximum heating rates of the order of 10 K/ms, again representative of LOF conditions: all these experiments produced fuel failure under low mechanical constraint, the DEH experiments by using a quartz clad close to its melting point and the slower of the FD1 experiments by having no clad at the time of rapid swelling owing to clad meltoff. The FD1 experiments exhibiting fine-scale fragmentation were constrained by relatively cool clad ($\sim$ 1050 K) but the short fuel columns were axially constrained by spring-loaded end pieces that would lift under pressures of 2 bars. Fuel fragments were observed to come from the axial ends of the fuel column.

Because of the importance of fuel disruption modes to LMFBR accident analysis, a theoretical examination has been made of the fine-scale fragmentation experiments to determine the phenomena responsible for this behavior. Since the stresses required to fragment UO_2 below its melting point must be of the order of the ultimate tensile stress or the yield stress, it is natural to

suspect that an agent capable of producing such high stresses must be involved and must be able to produce fracture on a grain-size scale. The most likely candidate under these conditions is fission gas which is known to exist both within grains[6] and on grain boundaries[7] in the form of small bubbles. The problem of producing high stresses even with the existence of stress concentrations near crack tips suggests that non-equilibrium bubble dynamics[8] may play an important role. Before examining what features of bubble dynamics need to be modeled, it is necessary to appreciate how the fragmentation could proceed even if high local stresses were available and to determine some necessary conditions that must be fulfilled.

2. CONDITIONS FOR CRACK ADVANCE

2.1 Stress Criterion

Bubbles can exist both within and on the surface of fuel grains and both bubble fields will be considered in the discussion which follows.

To establish some nomenclature, consider the penny-shaped crack around a spherical bubble in Figure 1.

If the gas pressure in the bubble is P_g, then a mechanical force, P_x, is exerted by the gas on the surrounding fuel matrix at the surface of the bubble:

$$P_x = P_g - \left(P_H + \frac{2W_s}{r_b} \right) \tag{1}$$

where P_H is the hydrostatic pressure and W_s is the energy per unit area required to create a free surface. The force is compressive
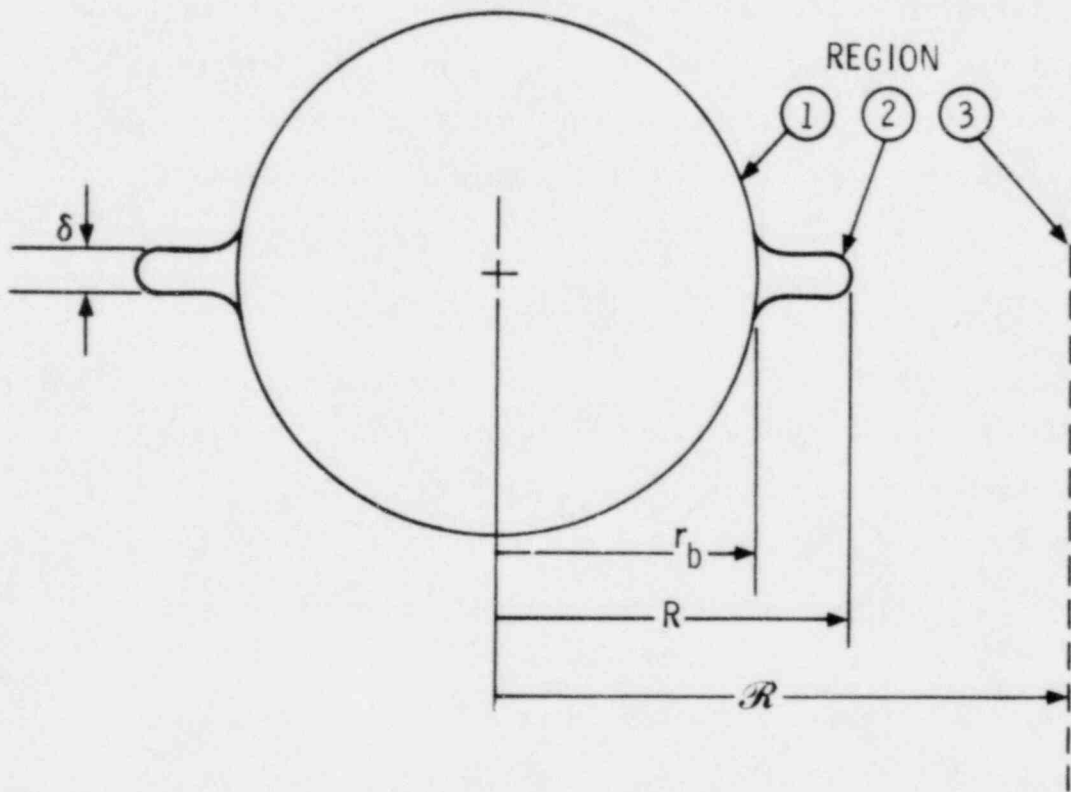
FIGURE 1. BUBBLE WITH PENNY SHAPED CRACK

if P_x is positive. If the bubble is on a grain boundary the free surface energy is reduced by an amount corresponding to that already expended to create the grain boundary

$$2W_s = 2\gamma_s - \gamma_{gb}$$ (2)

where γ_s is the free surface energy and γ_{gb} is the grain boundary energy. Within a grain W_s is equal to γ_s.

Gruber et al[9] have considered the loss of grain boundary adhesion consequent upon rapid heating of a set of grain boundary bubbles by calculating the excess pressure needed to yield the fuel matrix at the crack tip taking account of the stress concentration in that region. For a grain boundary areal coverage fraction of 0.5, the relationship is essentially

$$P_x \geq \frac{\sigma_y}{f}$$ (3)

where f is the stress concentration factor, and σ_y is the yield stress. The question of the stress required to part the lattice is related to the mechanism involved. For fully brittle failure, the local stress must be the ultimate tensile stress. When the material is fully ductile, plastic deformation will occur, in the absence of work hardening, at the yield stress although there may still be reasons for using the UTS for the fracture condition.[10] However for temperatures above 2000 K, the UTS and yield stress of UO_2 both have decreased considerably from their lower temperature values and approach values somewhat less than 5×10^7 N/m^2. Gruber uses a value of 3.5×10^7 N/m^2 from the work of Bard and Dutt.[11] Gruber also notes that the minimum

value of the stress concentration factor corresponds to that for a a sphere and the maximum to that for an ellipsoidal crack[12] so that

$$2 < f < 3.2.$$

These values suggest that the fracture stress criterion for P_x should be very approximately:

$$P_x \gtrsim 10^7 \quad N/m^2 \tag{4}$$

Notice that the requirement of non-zero excess pressure dictates a non-equilibrium treatment of bubble growth.

2.2 Differential Energy Criterion

Finnis[13] has noted that a fracture stress criterion alone is inadequate and that consideration must be given to thermodynamic criteria of the type first applied by Griffith[14] to unstable crack propagation in a fully brittle manner. The standard Griffith approach is to consider the surface energy requirement to incre- ment the crack dimension and to assume that the energy is supplied from a release of elastic strain energy in the whole medium and from contributions of potential energy from changes in the points of application of the stress system Since the strain plus poten- tial energy generally have a different dimensional dependence on the crack length than that of the surface energy, an unstable crack length can be defined under constant load conditions.

For a gas bubble with large positive overpressure, however, the strain energy and potential energy changes make very unequal contributions.

Bullough and Perrin[15] have developed an expression for the elastic energy of a body containing a spherical dilation center

subject to an excess pressure, P_x. This expression is

$$E_{el} = \frac{\pi}{\mu} \left[\frac{r_o^3 (P_x - P_H)^2}{2} - \frac{2(1-2\nu)}{(1+\nu)} r_o^3 P_x P_H + \frac{(1-2\nu)}{(1+\nu)} P_H^2 L^3 \right] \quad (5)$$

where the bubble radius r_o is that attained before the elastic medium is deformed by boundary forces, i.e., before loading, ν is Poisson's ratio, μ the shear modulus, and L is the macroscopic extent of the medium. If the hydrostatic pressure remains constant, the third term does not contribute to changes in E_{el}. Furthermore, for P_x of the order 500 bars and P_H of the order 2 bars, the second term is negligible in relation to the first. Under these conditions the expression reduces to

$$E_{el} = \frac{\pi P_x^2 r_o^3}{2\mu} \quad . \quad (6)$$

To the same approximation the radial displacement at the bubble surface is given by

$$U_r = \frac{P_x r_o}{4\mu} = \Delta r_{elastic} \quad (7)$$

Differentiation of Eq. (6) can be manipulated to give the rate of energy change with crack extension assuming the strain field is unchanged by the presence of a small crack. However a rather more satisfactory procedure that better illustrates the source of the energy contributions is to consider Eq. (6) as an expression of the linear elastic approximation:

$$E_{el} = \frac{1}{2} P_x (V - V_o) \qquad (8)$$

where V_o is the bubble volume before loading and V is the bubble volume after loading.

Equation (7) gives:

$$V - V_o = \Delta V_{elastic} = 3 V_o \frac{\Delta r_{elastic}}{r_o} ,$$

so
$$V - V_c = \frac{3 V_o P_x}{4\mu} \qquad (9)$$

and
$$d(V - V_o) = \frac{3}{4\mu}(V_o\, dP_x + dV_o\, P_x). \qquad (10)$$

Differentiating Eq. (8) and using Eq. (10):

$$2dE_\ell = P_x \cdot \frac{3}{4\mu}(V_o\, dP_x + dV_o\, P_x) + (V - V_o)\, dP_x. \qquad (11)$$

This processs allows the effective, unloaded, bubble volume to increase as the crack extends (dV_o) and takes account of the consequent pressure decrease (dP_x).

Assuming crack advance occurs instantaneously, there is no time for adjustment of the bubble shape due to creep processes, although these are considered later, and the bubble radius will remain constant as the crack extends by dR (Figure 1).

Therefore for an ideal gas:

$$dP_x = dP_g$$

$$= - \frac{P_g}{V}\, dV. \qquad (12)$$

Inserting this in Eq. (11) and using Eq. (9) for $(V - V_o)$ gives:

$$2 \, dE_{el} = \frac{3 \, P_x}{4\mu} [P_x - 2 \, P_g] \, dV_{crack} \tag{13}$$

with $\frac{dV}{\zeta V_o} \sim 1$ and $\frac{V}{V_o} \sim 1$ and $dV_o = dV_{crack}$.

This result is negative showing that strain energy is released and is of order $P^2 dV_{crack}/\mu$.

The gas, expanding into the crack volume, does work equal to $P_g dV_{crack}$ which is bigger than dE_{el} by a factor $\frac{\mu}{P} \gtrsim 100$.

Consequently the differential energy criterion for crack advance becomes

$$- P_g \, dV_{crack} + 2W_s \, \frac{dV_{crack}}{\delta} \leq 0 \tag{14}$$

where δ is the crack opening displacement (COD) or crack height.

Therefore, for crack advance we must require

$$P_g \geq \frac{2W_s}{\delta} = P_{gcrit'} \tag{15}$$

that is

$$\left. \begin{array}{ll} \text{on grain boundaries} & \delta \cdot P_g \geq 2\gamma_s - \gamma_{gb} \\ \text{within grains} & \delta \cdot P_g \geq 2\gamma_s \end{array} \right\} \tag{16}$$

This condition appears to be more severe than the fracture stress criterion of Eq. (4) and is independent of the details of

the elastic strain field. Its relation to crack morphology is through the COD, δ.

Values of surface energies and COD are subject to considerable uncertainty. A few conclusions may be drawn, however, that do not depend strongly on these uncertainties.

Since γ_{gb} is a considerable proportion of γ_s, clearly the critical pressure for advance of intragranular cracks is several times higher than that for intergranular cracks.

In a bubble with pressure increasing, an increment of crack growth is experienced as soon as P_g gets infinitesimally larger than P_{gcrit}. A consequent decline of P_g will occur as the crack volume increases, but providing dP_g/dt is greater than zero from other processes such as bubble coalescence, the crack volume will continue to increase to maintain $P_g = P_{gcrit}$. As soon as dP_g/dt becomes negative, crack advance will cease and P_g will fall below P_{gcrit}. The behavior is quite unlike unstable crack propagation in the classic brittle sense because Eq. (14) is homogeneous (in fact independent) in the crack dimension.

Since the crack growth is a quasi-equilibrium phenomenon, it is unlikely that the crack can develop by simple cleavage of the lattice or grain boundary to a width of only one or two lattice constants characteristic of the "classic" type of brittle failure. Steady crack advance will allow time for mass transfer to adjust the geometry of the crack tip, and the mechanical stability condition on the grain boundary requires the half angle, θ, of crack opening to be $\cos^{-1}\left(\frac{\gamma_{gb}}{2\gamma_s}\right)$. Various values for the surface energies suggest θ is in the range 40 to 70°. Furthermore at

high stresses a small zone of plasticity may be expected around the crack tip giving quasi-brittle behavior but a COD larger than one or two lattice parameters.

In practice, of course, the two conditions (Eqs. (3) and (15)) are not incompatible. If the stresses around a sharp crack cause local yielding, the COD will increase so that the fracture condition is just satisfied. Because of the attendant uncertainties, a constant COD is used in the discussion which follows.

The preceding considerations suggest a rather stubby crack shape for small bubbles not unlike that shown in Figure 1. Grain boundary widths may be assumed to be of order 0.5 nm[17] (the lattice constant in UO_2 is 0.34 nm) and so a crack opening displacement in the region 1 to 3 nm may be expected. The values:

$$(2\gamma_s - \gamma_{gb}) = 0.25 \ Jm^{-2}; \quad \delta = 2nm$$

yield
$$P_{gcrit} \sim 1.25 \ 10^8 \ N/m^2$$

with a value perhaps five times higher for crack growth within grains. Because of the size range of δ, this calculation should only be applied for bubble radii larger than, say, 5 nm. It is also worth noting that for bubbles with radii of order 1 nm on grain boundaries, even equilibrium ($P_x=0$) pressures are of order 10^8 N/m^2. For such bubbles $r \approx \delta$ and the above analysis is inapplicable. Referring to the stress criterion $P_x \geq \sigma_y/f$, for an elliptical crack in tension, the stress concentration factor is of order[18]

$$f \sim \sqrt{\frac{r_b}{\delta}}$$

Thus $f \sim 2.2$ for such a crack with $r_b = 10.0$ nm and $\delta = 2$ nm.

The criteria for intragranular crack advance established so far are:

1. (Stress) $\qquad P_x \geq \dfrac{\sigma_y}{f} \qquad \sim 10^7 \text{ N/m}^2 \qquad$ (17)

2. (Differential energy requirement) $\qquad P_g \geq \dfrac{2W_s}{\delta} \qquad \sim 10^8 \text{ N/m}^2 \qquad$ (18)

For continuous crack advance it is also necessary that

$$\frac{dP_g}{dt} \text{ (coalescence and heating)} > 0 \qquad (19)$$

where P_g is calculated in a bubble dynamics calculation that ignores cracks.

2.3 Total Energy Criterion

The phenomenon of disruption must also be related to crack interlinkage between neighboring bubbles. This could be calculated in a bubble dynamics model by keeping track of crack advance as allowed by the above criteria. However the uncertainties inherent in both criteria and dynamics models, the random arrangement of bubbles on grain boundaries, and the random orientation of cracks around intragranular bubbles suggest that a criterion based on total energy may be sufficiently accurate and of more general applicability than a sophisticated crack growth calculation.

For this purpose assume that the bubble dynamics calculation proceeds in the absence of cracks, allowing P_g to exceed P_{gcrit}. The total energy that could be obtained by the gas expanding into a crack volume produced by a crack of height δ and extending half

the interbubble distance may be compared to the total surface energy requirement.

$$\text{Gas expansion work} = E_{gas} = \int_{V_o}^{V_f} p\, dV$$

For isothermal conditions

$$E_{gas} = nkT \quad \ln\left[\frac{V_o + 1/2A\delta}{V_o}\right] \tag{20}$$

where n is the number of gas atoms per bubble, A is the total crack surface area and T the absolute temperature.

$$A = 2\pi (\mathcal{R}^2 - r_b^2) \qquad \text{(see Figure 1)} \tag{21}$$

For intragranular bubbles the interbubble spacing $\mathcal{R}$, is given by an equivalent sphere dimension:

$$\frac{4}{3}\pi\mathcal{R}^3 = \frac{1}{C_b} \tag{22}$$

where C_b is the number of bubbles per unit volume. For the calculations reported later, the ratio $\mathcal{R}/r_b$ is in the range 2 to 3 in the fastest transients but is closer to 1.5 for more modest heating rates.

The calculations show that for bubbles on grain boundaries, when the crack growth criteria are approached, the bubble density is generally high giving, say, a 50% areal coverage.

For this case $\mathcal{R}^2/r_b^2 = 2$ and $\mathcal{R}/r_b = 1.4$. Therefore it appears generally easier to link up intergranular bubbles than

intragranular ones especially when the arbitrary orientation of cracks in the latter case is considered.

In Eq. (20) the argument of the logarithm may be written

$$1 + \frac{A\delta}{2V_o} = 1 + \frac{3}{4}\left(\frac{\mathcal{R}^2}{r_b^2} - 1\right)\left(\frac{\delta}{r_b}\right) \tag{23}$$

In even the fastest transients calculated later the bubble radius is many times larger than δ when $P_g \geq P_{gcrit}$ for both bubble fields. However for intragranular bubbles, the first term in brackets is then large enough to compensate and the right-hand side of Eq. (23) has a value considerably greater than unity. For other cases, fast transients for intergranular bubbles (the first bracket is around unity) and for slower transients (where the bubble radius is very much larger than the COD for both bubble fields) the right-hand side becomes $1 + \epsilon$ with $\epsilon \ll 1$.

In the latter case, Eq. (20) reduces to

$$E_{gas} = \frac{nkT\ A\delta}{2V_o} = \frac{P_g\ A\delta}{2} . \tag{24}$$

The surface energy required is

$$E_s = AW_s \tag{25}$$

and so cracks will interlink when $E_{gas} \geq E_s$, or

$$P_g \geq \frac{2W_s}{\delta} . \tag{26}$$

This is exactly the condition (Eq. (18)) for crack advance. This result implies that if the product of the terms in brackets on the right-hand side of Eq. (23) is less than about 0.3, there is enough potential energy in the gas to link the cracks, provided Eq. (26)(18) is satisfied. As has been briefly mentioned, this is not the case for intragranular cracks in very fast transients (~ 100 K/ms), but should just about be satisfied in other circumstances for both bubble fields.

Remember that this treatment of total energy requirement is only approximate and does not correspond to physical reality as far as the dynamics of crack advance are concerned. The derivation of Eq. (24) essentially regards the crack volume as a differential increment, not a bad approximation when large bubbles are close together. For other circumstances the energy requirement should be obtained by equating the full form of Eq. (20) to Eq. (25).

Note that no terms corresponding to crack nucleation have been included in the above energy formulation, as has been done by DiMelfi and Dietrich.[19] On grain boundaries, at least, there is no reason to treat cracks as either pre-existing defects or as the result of dislocation pile-up when bubbles can freshly arrive at the boundary from the interior of a grain and exist there in a state of mechanical disequilibrium with the lattice. In this case the flow of vacancies along the grain boundary to the equatorial region of the bubble[20] will ensure that an incipient penny-shaped crack exists. The energy for moving vacancies into the compressive radial stress field at the bubble surface is supplied by the potential energy of the contained gas.

2.4 Creep Conditions

2.4.1 Stress States

Consideration of the effects of mass transport at the crack is now appropriate. When the lattice is held in compression, the local vacancy concentration is decreased below the thermal equilibrium value by the factor $\exp\left(-\dfrac{P_x \Omega}{kT}\right)$ where P_x is a (positive) radial compressive stress, here identified with the mechanical excess bubble pressure, Ω is the volume of a vacancy, and T the temperature. If the stress varies locally, there will be a diffusive vacancy flux proportional to the concentration gradient (Flux $= -D\,\dfrac{\partial c}{\partial x}$). The stress field around the crack will be complex and the following discussion only accounts for the gross features.

Three regions of differing stress state can be identified (Figure 1):

Region 1   At the bubble surface:

$$P_{x1} = P_g - \frac{2W_s}{r_b} \tag{27}$$

P_{x1} is positive during transients owing to heating and coalescence.

Region 2   Near the crack tip:

$$P_{x2} = P_g - \frac{2W_s}{\delta} \; : \quad P_{x2} < P_{x1} \text{ because } r_b > \delta \tag{28}$$

$$P_{x2} = 0 \qquad\qquad \text{when } P_g = \frac{2W_s}{\delta} \text{ -- crack growing}$$

$$\text{and } P_{x2} < 0 (\text{tensile}) \qquad \text{when } P_g < \frac{2W_s}{\delta} \text{ -- crack stationary} \tag{29}$$

Once again this depends upon the crack advance criterion of Eq. (18).

<u>Region 3</u>   Midway between bubbles:

If this region is assumed stress-free, then the vacancy concentration may be maintained at the thermal equilibrium value C_v^{eq}. When very many strong sinks exist, as during a heating transient, it will in general not be possible to maintain the thermal equilibrium concentration. The later discussion of bubble dynamics allows C_v^{eq} to be modified, but for present purposes this will be ignored.

A vacancy flux should be expected to occur from Region 2 to Region 1 at all times ($P_{x2} < P_{x1}$ always) and from Region 2 to Region 3 while the crack is stationary ($P_g < 2 W_s/\delta$). The first of these processes transfers volume from the crack tip to the bubble but does not change the total volume available to the n gas atoms present; whereas the second process removes volume from the crack tip and therefore tends to increase the bubble pressure. Furthermore, while the crack is growing, P_g is maintained equal to $2 W_s/\delta$ and $P_{x2} = 0$. The vacancy flow outwards from the crack then ceases.

When no crack is present, vacancies flow from Region 3 to the bubble surface and constitute the only way by which bubbles effectively gain volume and tend to mechanical equilibrium.

It is now convenient to consider the bubble fields separately.

2.4.2 Intergranular Cracks

It is expected that because surface diffusion and grain boundary diffusion processes are much more rapid than bulk diffusion, vacancies are expected to predominantly flow between Regions 2 and 3 through the grain boundary and between Regions 1 and 2 through the surface of the crack.

2.4.2.1 Grain Boundary Diffusion

Hull and Rimmer[20] were the first to consider grain boundary void growth by grain boundary diffusion, and their formulation has been used by DiMelfi and Dietrich[19] in considering the vacancy flux opposing crack growth in UO_2. An additional boundary condition was imposed by Speight and Harris[21] to account for vacancy sinks throughout the diffusion volume. This type of boundary condition can be used to approximate, on the average, the effect of the total vacancy source from edge porosity.

The diffusion equation is solved[21,22] in an annular section of the grain boundary whose inner radius, for purposes of this report, is R, the crack radius, and whose outer radius is $\mathcal{R}$ (Figure 1).

The boundary conditions are

$$C_v(\mathcal{R}) = C_v^{eq}$$

$$C_v(R) = C_v^{eq} \exp\left(-\frac{P_{x2}\Omega}{kT}\right) \qquad \begin{array}{l} (P_{x2} < 0 \\ \text{when} \\ \text{tensile)} \end{array} \qquad (30)$$

$$\left.\frac{dC_v}{dr}\right|_{\mathcal{R}} = 0,$$

and the diffusion equation is

$$D\,\frac{1}{r}\,\frac{d}{dr}\left(\frac{rdC_v}{dr}\right) + S = 0 \qquad (31)$$

where D is the vacancy diffusion coefficient and S is the uniform volumetric source giving the steady-state solution. The equilibrium concentration is modified in numerical calculations by a

22

multiplicative constant that adjusts for the competition for vacancies and the consequent vacancy depletion in the grain boundary.

The solution gives

$$\frac{dC_v}{dr}\bigg|_R = \frac{2C_v^{eq} P_{x2} \Omega}{RkT} \cdot \frac{\left[1 - \left(\frac{R}{\mathscr{R}}\right)^2\right]}{\left[\ell n\left(\frac{\mathscr{R}}{R}\right)^2 - \left(1 - \left(\frac{R}{\mathscr{R}}\right)^2\right)\right]} \tag{32}$$

where the exponent in the boundary condition, Equation 30, has been linearized.

The flux then gives a volume flow rate across an area of width w and radius R of

$$\dot{V}_{gb} = 4\pi w C_v^{eq} D \Omega^2 \frac{P_{x2}}{kT} H_{gb} \tag{33}$$

if the volume of each vacancy is Ω. H_{gb} is a geometric factor

$$H_{gb} = \left[1 + \frac{\ell n \left(\frac{R}{\mathscr{R}}\right)^2}{\left(1 - \left(\frac{R}{\mathscr{R}}\right)^2\right)}\right]^{-1} . \tag{34}$$

If $\mathscr{R} \sim 1.4\ r_b$ and $R\ 1.01\ r_b$, $H_{gb} = 2.7$; if $R = 1.2\ r_b$, $H_{gb} = 1.2$. Clearly H_{gb} is of order unity for a short crack and, if by convention the product $\Omega C_v^{eq} D$ is replaced by D_{gb},

$$\dot{V}_{gb} = -4\pi w D_{gb} \frac{P_{x2}\Omega}{kT} . \tag{35}$$

For stable cracks P_{x2} is negative so that $\dot{V}_{gb}$ represents a volume flow in the positive r direction, away from the crack tip.

2.4.2.2 Crack Surface Diffusion

Vacancies can diffuse through a surface layer approximately
one lattice spacing thick, λ. It is perhaps easier to imagine
uranium ions diffusing in the surface layer towards the crack
tip. The solution is obtained by direct integration of Eq. (31),
omitting the source term and using the boundary conditions.

$$C_v(R) = C_v^{eq} \exp\left(- \frac{P_{x2}\Omega}{kT}\right)$$

$$C_v(r_b) = C_v^{eq} \exp\left(- \frac{P_{x1}\Omega}{kT}\right) . \tag{36}$$

The volume flux at the crack tip becomes

$$\dot{V}_{sp} = 4\pi\lambda D_s C_v^{eq} \ (P_{x2} - P_{x1}) \ \frac{\Omega^2}{kT} \cdot H_{sp} \tag{37}$$

where D_s is the surface diffusion coefficient.

Two crack surfaces are included, the exponentials have been
linearized, and the factor H is now

$$H = - \frac{1}{\ln\left(\frac{r_b}{R}\right)} = [\ln a]^{-1} \tag{38}$$

where $R = ar_b$.

For a short crack, a may be written as $(1+\epsilon)$ with $\epsilon \ll 1$.
Then H may be expanded in powers of ϵ to give

$$H \approx \epsilon^{-1}.$$

This relationship is approximately true even for cracks extending three quarters of the way to the point midway between bubbles when the coverage fraction on the grain boundary is 50%.

Consequently the vacancy flow tending to impart spherical shape to the bubble gives a volume flow rate

$$\dot{V}_{sp} = \frac{4\pi}{\epsilon} \lambda D_s C_v^{eq} (P_{x2} - P_{x1}) \frac{\Omega^2}{kT} \tag{39}$$

Since $P_{x2} < P_{x1}$, always, $\dot{V}_{sp}$ represents a volume flow to negative r, i.e., from the crack tip to the bubble.

Griesmeyer and Ghoniem[23] give an expression for $C_v^{eq}\Omega$ for both stoichiometric and hyperstoichiometric fuel. In the stoichiometric case:

$$C_v^{eq}\Omega = 2 \exp\left(-\frac{3.8 \ 10^4}{T}\right). \tag{40}$$

The surface diffusion coefficient D_s can be represented[24,28] as

$$D_s = 3.5 \exp\left(-\frac{4.5 \ 10^4}{T}\right) \qquad m^2/s \tag{41}$$

and therefore in Eq. (39) the volume flux may be written

$$V_{sp} = \frac{28\pi}{\epsilon} \frac{\lambda\Omega}{kT} (P_{x2} - P_{x1}) \exp\left(-\frac{8.3 \ 10^4}{T}\right) \qquad m^3/s. \tag{42}$$

DiMelfi and Dietrich[19] suggest a value for wD_{gb} of

$6.3 \ 10^{-15} \ \exp\left(-\frac{3.5 \ 10^4}{T}\right) m^2/s$ and Reynolds and Burton[17] recently measured a value of $6.9 \ 10^{-16} \ \exp\left(-\frac{2.9 \ 10^4}{T}\right) m^2/s$ (assuming $w = 0.5$ nm as in their work). In the temperature range 2500 K to 3000 K both these formulations are closely equivalent and agree exactly at 2700 K. The measurement of Reynolds and Burton will be used in this work because uncertainties are quoted for D_{gb} which imply (assigning no uncertainty to w) that

$$w D_{gb} = 6.9 \left(\begin{array}{c} \times 5 \\ \div \end{array}\right) \times 10^{-16} \ \exp\left[-\frac{(2.87 \pm 0.96) \times 10^4}{T}\right]. \quad (43)$$

Equation (35) for the grain boundary volume flux is then

$$\dot{V}_{gb} = -2.8 \ 10^{-15} \ \pi \ \frac{P_{x2} \ \Omega}{kT} \ \exp\left(-\frac{2.9 \ 10^4}{T}\right) \quad m^3/s \quad (44)$$

While a crack is stationary the total rate of crack elimination by creep processes will be

$$\dot{V}_T = \left|\dot{V}_{sp}\right| + \left|\dot{V}_{gb}\right|. \quad (45)$$

For $\varepsilon = 0.1$ typical values near the time of peak internal pressures calculated in the transients to follow for stable (i.e., $P_g < 2 \ W_s/\delta$) cracks, give:

$$\left|\dot{V}_{gb}\right| \sim 5 \left|\dot{V}_{sp}\right| \quad \text{at 2700 K and}$$

$$\left|\dot{V}_{gb}\right| \sim \left|\dot{V}_{sp}\right| \quad \text{at 2900 K.}$$

The relative increase in $\left|\dot{V}_{sp}\right|$ at higher temperatures arises from the much greater "effective" activation energy for surface diffusion in Eq. (42) compared with that in the grain boundary in Eq. (44). Both values are, however, subject to large uncertainties, larger in fact than Eq. (43) alone indicates.

2.4.3 Intragranular Cracks

The only vacancy flows will be through the lattice or on the crack surface. Assuming that in addition to the bulk flow to the whole bubble calculated for bubble dynamics the only important contribution is the diffusion along crack surfaces, then Eq. (42) for $\dot{V}_{sp}$ applies without further change. Note that $\dot{V}_{sp}$ does not change the bubble volume but only tends to impart spherical shape to the defect.

2.4.4 Mass Transfer Criterion

DiMelfi and Dietrich[19] have suggested that volume can be removed from the crack tip by vacancy diffusion after the manner of Hull and Rimmer.[20] However the present analysis suggests that although the order of magnitude of this effect is about correct, it may be more physically realistic to imagine vacancy diffusion in the crack surface from crack tip to bubble at all stages of crack growth and from crack tip to the between-bubble region via the grain boundary while the crack is stationary (i.e., existing but with $P_g < \dfrac{2W_s}{\delta}$. While the crack is growing, the grain boundary diffusion should cease (Eqs. (35), (29)). Even if this last situation is not exactly true (the crack tip curvature is only of order δ), the approximate equivalent magnitudes of the

27

grain boundary and crack diffusion effects for stationary cracks suggest that the grain boundary contribution is smaller than the crack surface contribution while the crack is actually growing. In the calculations to follow only crack surface diffusion is included.

Whenever P_g exceeds P_{gcrit}, instantaneous crack growth will restore P_g to equal P_{gcrit}. While P_g has a tendency to increase, this situation will be maintained.

Factors tending to increase P_g will be principally coalescence and to some extent heating, and factors decreasing P_g will be bulk vacancy diffusion and other creep processes. Dislocation creep[25] greatly enhances the bubble growth rate at around 2500 K and high internal pressure.

Since the crack surface diffusion does not affect the total volume, in the absence of crack growth

$$\dot{P}_g = \dot{P}_g \text{ bubble dynamics.} \tag{46}$$

The rate of crack volume extension that maintains $P_g = P_{gcrit}$ when $\dot{P}_g$ (bubble dynamics) > 0 is,

$$\dot{V}_{crack} = \frac{V}{P_g} \dot{P}_g . \tag{47}$$

Therefore to continuously heal cracks it is essential that

$$|\dot{V}_{sp}| \geq \frac{V}{P_g} \dot{P}_g \text{(bubble dynamics)}. \tag{48}$$

The dominant dependence in Eq. (42) for $\dot{V}_{sp}$ is on temperature and in general $\dot{V}_{sp}$ will increase as the temperature rises.

2.5 Overall Disruption Criteria

All the following conditions must all be met in order for the UO_2 matrix to lose cohesion by the extensive growth of cracks on a grain-size scale:

1. $P_{x1} \geq \dfrac{\sigma_y}{f}$ stress condition   Eq. (3)

2. $P_g \geq \dfrac{2W_s}{\delta} = P_{gcrit}$ differential energy condition   Eq. (18)

3. $\dot{P}_g$ (bubble dynamics) > 0 pressure increasing   Eq. (19)

4. $E_{gas} \gtrsim E_{surface}$ total energy condition   Eqs. (20-25)

5. $|\dot{V}_{sp}| < \dfrac{V \dot{P}_g}{P_g}$ (bubble dynamics)   Eq. (48)

                            mass transfer condition

Generally Condition 1 is much less precise than Condition 2. For calculational purposes it is much preferable to have a condition that depends on P_g rather than one depending on P_{x1} because P_{x1} is more sensitive to calculational uncertainties. This arises because $2W_s/r_b$ is an appreciable fraction of P_g and therefore P_{x1} is the difference of two quantities, similar in magnitude. Moreover, $2W_s$ itself is a small difference of two larger quantities for bubbles on grain boundaries (see Section 5.1 for a numerical example).

For large, closely-spaced bubbles, Condition 4 reduces to Condition 2. Condition 3, of course, is implied by both 2 and 5 and is therefore not an independent condition.

3. REQUIREMENTS OF THE BUBBLE DYNAMICS MODEL

The conditions above depend strongly on effects that influence the bubble pressure. Clearly coalescence, vacancy-flux limited bubble growth, other creep relaxation mechanisms, and gas atom sweep-up should be included. The model should account for both intragranular and intergranular gas and should couple the bubble fields through a gas release mechanism. Some of the phenomena have been studied for many years and are reviewed by Olander.[26]

3.1 Intragranular Bubbles

The treatment here follows the straightforward calculational framework of the Harwell NEFIG[27] model with important innovations introduced initially by Ostensen in the FISGAS[28] code.

Gas is initially partitioned[27] between single gas atoms and small bubbles. The bubbles are of uniform size and move by surface diffusion both randomly[29,30] and by biased motion in a temperature gradient.[31] Single gas atoms both diffuse to bubbles and are also swept up[27] by bubble motion both biased and random. As in NEFIG the single gas atoms carry two vacancies[27] each. Bubble interactions in the delta-function size distribution are modeled as $\alpha\pi(2r_b)^2$ with α as an adjustable parameter. The vacancy flux to the bubbles[8] is source-limited as given by the approximate rate theory expression introduced by Matthews and Wood.[27] Gas in bubbles is released to grain boundaries by both coherent motion of the bubble cloud and by random bubble motion. Grains are treated as spherical in shape and the reduced Van der Waals equation-of-state is used throughout.

Ostensen found[4] that some features of the gross swelling observed in the FD1 experiment could be explained by the introduction of bubble relaxation by power law creep at high temperatures and used a thin cylinder approximation. Recent observations[25] of enhanced power law creep in UO_2 above 2673 K suggest that activation of dislocation movements should be added to creep by bulk point defect diffusion of the type already included in the present model. The enhanced creep in the present calculations is accounted for with a thick-walled-sphere macroscopic creep formula (see Appendix I) relating the creep rate to the bubble excess pressure acting over a distance given by the inter-bubble spacing. Relaxation of all creep restraint is allowed at temperatures exceeding the liquidus.

The equations used in the intragranular model are as follows:

For a bubble of radius r the velocity in a temperature gradient is given by

$$v = \frac{3 \lambda D_s \, |\nabla T| \, Q_s^*}{rT^2 k} \tag{49}$$

where Q_s^* is the heat of transport.
The gas pressure is

$$P_g = \frac{nkT}{\frac{4}{3}\pi r^3 - Bn} \tag{50}$$

where n is the number of gas atoms per bubble and B is the Van der Waals constant ($8.5 \; 10^{-29} \; m^3$).

The bubble excess pressure is

$$P_x = P_g - \left(P_H + \frac{2\gamma_s}{r}\right).$$ (51)

The rate of accumulation of gas atoms in a bubble is

$$\dot{n} = \dot{n}_1 + \dot{n}_2$$

with $\dot{n}_1 = -\dot{C}_g/C'_b$ (from single gas atoms)

(52)

and $\dot{n}_2 = -n\dot{C}_b/C'_b$ (from bubble coalescence)

where C_g is the concentration of single gas atoms and C_b is the concentration of bubbles. Primed quantities denote those corrected for swelling, i.e.,

$$C'_b = \frac{C_b}{1 + \frac{4}{3}\pi r^3 C_b}$$ (53)

where C_b refers to the original unswollen unit volume. The bubble concentration changes because of coalescence events due to both biased (first term) and random (second term) motion.

$$\dot{C}'_b = -4\pi\, \alpha r^2 v {C'_b}^2 - \frac{12\lambda^4 D_s {C'_b}^2}{r^3}.$$ (54)

The gas atom concentration changes owing to sweep-up by bubbles (first and second terms) and by diffusion to bubbles (third term):

$$\dot{C}_g = - \pi r^2 v C_g C_b' - \frac{6\lambda^4 D_s C_g C_b'}{r^3} - 4\pi r D_g C_g C_b' \qquad (55)$$

where D_g is the single (Xe) atom diffusion co_fficient.

The bubble radius changes in response to coalescence (first term), to vacancies swept up with gas atoms[27] (second term), to vacancies diffusing through the lattice (third term) and to activation of dislocations (fourth term)

$$\dot{r} = - \frac{r\dot{C}_b'}{3C_b'} + \frac{\Omega \dot{n}_1}{2\pi r^2} + \frac{D_u}{r\Theta} \frac{P_x}{kT} \Omega + \dot{r}_{DCRP} \qquad (56)$$

where D_u is the uranium vacancy-diffusion coefficient and Θ is the factor introduced by Matthews and Wood[27] to account for vacancy depletion in the lattice.

$$\Theta = 1 + \frac{d}{3} \sqrt{\pi r \, C_b'} \qquad (57)$$

where d is the grain diameter.
The fourth term in $\dot{r}$ is given (Appendix I) by

$$\dot{r}_{DCRP} = \kappa \frac{r_{eff}^3}{r^2} \left(\frac{3}{2\nu}\right)^\nu \left[\frac{P_x}{\left(\frac{r_{eff}}{r}\right)^{3/\nu} - 1} \right]^\nu \qquad (58)$$

with

$$r_{eff}^3 = \frac{3}{4\pi \, C_b'} = \mathscr{R}^3 . \qquad (59)$$

This choice of creep relaxation length is chosen to accord with the assumption that the interbubble region is largely stress free. Although this assumption is certainly too simple, a proper treatment of creep relaxation of a random array of dilation centers represents a formidable problem.

The uniaxial creep rate is

$$\dot{\varepsilon} = \kappa \, \sigma^{\nu} \tag{60}$$

Although the major part of the gas release is by biased bubble motion, there is a possibility of significant contributions to the intergranular bubble population early in a transient coming from random bubble motion near the grain edge. Gruber[24] has modeled this in the FRAS code and his procedure is followed here.

$$f_{release} = \max(0, f_{random}, f_{bias} - \frac{f}{2} \, random) \tag{61}$$

where the f_i are release fractions.

$$\dot{f}_{bias} = \frac{3h(2d - h)v}{2d^3} \cdot \frac{nC_b'}{C_o} \tag{62}$$

where C_o is the total gas atom concentration

$$C_o = C_g + nC_b \tag{63}$$

and h is the overlap distance between the grain and the bubble cloud.

$$\dot{h} = -v \text{ and } h(t=0) = d \tag{64}$$

$$f_{random} = \frac{12x}{d^2} \left(\frac{d}{\sqrt{\pi x}} - 1 \right) \frac{nC_b'}{C_o} \tag{64}$$

$$\text{and} \qquad \dot{x} = \frac{3\lambda^4 D_s}{2\pi r^4} \tag{65}$$

The term $f_{release}$ represents only the release to the grain boundaries. Total volume swelling can be obtained by multiplying the swelling in the gas containing part of a grain (the overlapping spheres) by the fractional overlap volume.

$$S_{intra} = \frac{4}{3}\pi r^3 C_b \cdot \frac{h^2(3d - h)}{2d^3} \tag{66}$$

When the swelling is large, the way to correct d for the distortion in part of a grain becomes unclear and Eqs. (62) and (66) are only approximate.

3.2 Intergranular Bubbles

In the present calculations gas bubbles arriving at the grain boundary are assumed to tend to equilibrium by vacancy diffusion along the grain b undary.[20,21] The bubbles move about[28] on the two-dimensional grain surface by random and temperature gradient biased[28] motion, coalesce, and develop overpressures. The number of bubbles is calculated by integrating the arrival rate of bubbles that do not coalesce on arrival together with the coalescence

terms until the areal coverage fraction is, say, 50%.[33] One-third
of the grain boundary area is excluded from the calculation on the
assumption that this area represents well-connected porosity and
leads to the immediate release of gas impinging on it. After 50%
coverage is attained in the remaining area, the number of bubbles
is calculated by continuing to follow the growth of the bubbles
together with assuming the immediate release of newly-arrived gas
to maintain the constant coverage fraction. The boundary bubbles
are considered to be spherical.

The equations that are used are as follows:

The coverage fraction, Q_a, is

$$Q_a = \frac{2N \; r_B^2}{0.67 \; d'^2} \tag{67}$$

where N is the actual number of bubbles on the grain boundary of
area one-half the total (spherical) grain area. This accounts for
the predominantly biased component of intragranular bubble release
to the boundary, and the further factor of 0.67 roughly accounts
for the connected porosity as discussed above. Grain diameters
are corrected for swelling (primes).

A fraction Q_b of intragranular bubbles, incident on the
boundary, coalesce on arrival with existing intergranular bubbles
according to a cross section:

$$Q_b = \frac{2N}{0.67 \; d'^2} \left(r_B + r \right)^2 \; ; \; Q_b \leq 1 \tag{68}$$

where r_B is the radius of an intergranular bubble.

36

The temperature-gradient-biased motion leads to a bubble velocity given essentially by Eq. (49) so that

$$v_B = v \cdot \frac{r}{r_B} \cdot \frac{2}{\pi} \qquad (69)$$

where the factor $2/\pi$ gives the average projection of the temperature gradient along the grain surface. The number of intragranular bubbles arriving at the grain surface in unit time that contributes to the intergranular bubble field is simply

$$\dot{n}_{bB} = 0.67 \frac{C_o V}{n} \dot{f}_{release} \qquad (70)$$

where V is the unswollen grain volume.

Consequently the direct addition of intragranular bubbles to the number of intergranular bubbles is

$$\dot{N}_1 = (1 - Q_b) \dot{n}_{bB} . \qquad (71)$$

Coalescence among bubbles in the intergranular field occurs by temperature biased motion and by random motion on the two-dimensional surface,

$$\dot{N}_2 = - \frac{N^2}{0.67 \, d'^2} \left[\frac{4\alpha}{\pi} r_B v_B + \frac{18 \, \lambda^4 D_s}{\pi \, r_B^4} \right] . \qquad (72)$$

The same coalescence parameter, α, is used as in the intragranular calculation. Equation 72 is derived in Appendix II.

While $Q_a < 0.5$,

$$\dot{N} = \dot{N}_1 + \dot{N}_2 \tag{73}$$

and when $Q_a \geq 0.5$,

$$N = 0.67 \times \frac{0.5\ d'^2}{2\ r_B^2} . \tag{74}$$

The number of gas atoms per intergranular bubble, n_B, is calculated by sharing equally among the N bubbles, the number of newly-arrived atoms (first term) and the coalescence correction (second term):

$$\dot{n}_B = \frac{1}{N} (n\ \dot{n}_{bB} - n_B\ \dot{N}_2);\ Q_a < 0.5$$

and

$$\dot{n}_B = \frac{1}{N} (n\ \dot{n}_{bB}\ 0.5 - n_B \dot{N}_2);\ Q_a \geq 0.5 . \tag{75}$$

The gas pressures are

$$P_{gB} = \frac{n_B\ kT}{\frac{4}{3}\pi r_B^3 - Bn_B} , \quad \text{and} \tag{76}$$

$$P_{xB} = P_{gB} - \left(P_H + \frac{2\gamma_s - \gamma_{gB}}{r_B} \right) . \tag{77}$$

Bubbles grow according to coalescence among intergranular bubbles (first term), impact coalescence from arriving intragranular bubbles (second term), grain boundary vacancy diffusion (third term) and by power law creep (fourth term):

$$\dot{r}_B = -\frac{r_B \dot{N}_2}{3N} + \frac{r_B^3 \dot{n}_{bB}}{3N\, r_B^2}\xi + \frac{wD_{gB}}{r_B^2}\frac{P_{xB}\Omega}{kT}H + \dot{r}_{BCRP} \qquad (78)$$

where $\quad \xi = Q_b \quad$ for $Q_a < 0.5$

$\qquad\qquad \xi = 0.5$ for $Q_a \geq 0.5$

and $\qquad H = \dfrac{g}{\dfrac{\ln Q_a}{(Q_a - 1)} - 1}$. $\qquad\qquad\qquad\qquad$ (79)

The factor g is included to enable the vacancy concentration away from bubbles to be reduced below the thermodynamic equilibrium value. This approximates the effect of lattice depletion owing to competition for vacancies between the large number of intragranular sinks and for the close spacing of intergranular bubbles. This factor has been included as a parameter and thus the intragranular and intergranular bubble fields are not analytically coupled via the grain-boundary-vacancy source strength. A value of g in the region of 0.1 has been used, and has the effect of approximately doubling the intergranular pressures in all the calculated transients while having little effect on other quantities. The same factor g is applied to the vacancy flux formula for $\dot{V}_{sp}$ along crack surfaces on grain boundaries.

The macroscopic creep term in Eq. (78) is given by Eq. (58) with r replaced by r_B and P_x replaced by P_{xB}.

Intergranular swelling is given simply by

$$S_{inter} = \frac{8N \, r_B^3}{d^3} \tag{80}$$

and the total swelling by

$$S = S_{inter} + S_{intra}. \tag{81}$$

4. CALCULATION FRAMEWORK

The calculations reported here were carried out using a multi-zone representation of the fuel cross section in the radial direction. Although fission gas calculations have often been performed only for the unrestructured fuel region, recent measurements by Randklev[34] and earlier measurements by Scott et al[35] have shown a "tail" to the gas distribution extending through the equiaxed region. Moreover observations by Cano[36] on Fül swelling show that important effects are not confined to the unrestructured zone. Heat transfer calculations[5,4] suggest also that in the FD1 experiments which dispersed, peak temperatures at disruption time occurred in the region of 0.6 to 0.7 radius ratio. For all of these reasons the present calculations use an inner radius corresponding to about 0.1 radius ratio.

4.1 Initial Conditions and Parameter Values

The initial conditions concern the gas distribution, gas partition between single atoms and bubbles, and bubble size. In general, little attempt has been made in the discussion which

follows to find optimum sets of parameters and previously suggested "reasonable" numbers have been used almost everywhere.

Radial gas distributions have been taken from the work of Randklev[34] and Scott et al[35] with total gas content according to the Dutt[37] correlation which assumes gas exists in a uniform distribution in the unrestructured region alone. The use of this radial distribution does not have a significant effect on the results unless radial variations in material properties stemming, for example, from a radial variation in stoichiometry are also included. This has not been done in the calculations reported here. The gas partition has been chosen so that about 30% of the gas atoms are in bubbles and 70% as interstitials with bubble concentrations in the range 10^{24}-10^{25} m^{-3} as measured by Baker[38] and used in NEFIG.[27] The bubble size is initially small[38] with a radius of 0.5 nm and containing 5.5 Xe atoms giving mechanical equilibrium at about 1600 K. Values of principal parameters used are given in Table 1.

4.2 Preliminary Calculations

Before applying the above model to crack growth phenomena, the basic handling of bubble dynamics was checked by comparison between calculations and the gas release data of FGR39, one of the HEDL gas release experiments,[7] and the fuel swelling data in the Sandia Laboratories FD1 experiments.[8] Figures 2 to 5 show the comparisons between data and calculation. FGR39 gas release is underpredicted by 35% late in the transient although of this deficit some 10% to 12% can be accounted for residing on grain boundaries. The calculation does not reproduce the early sudden
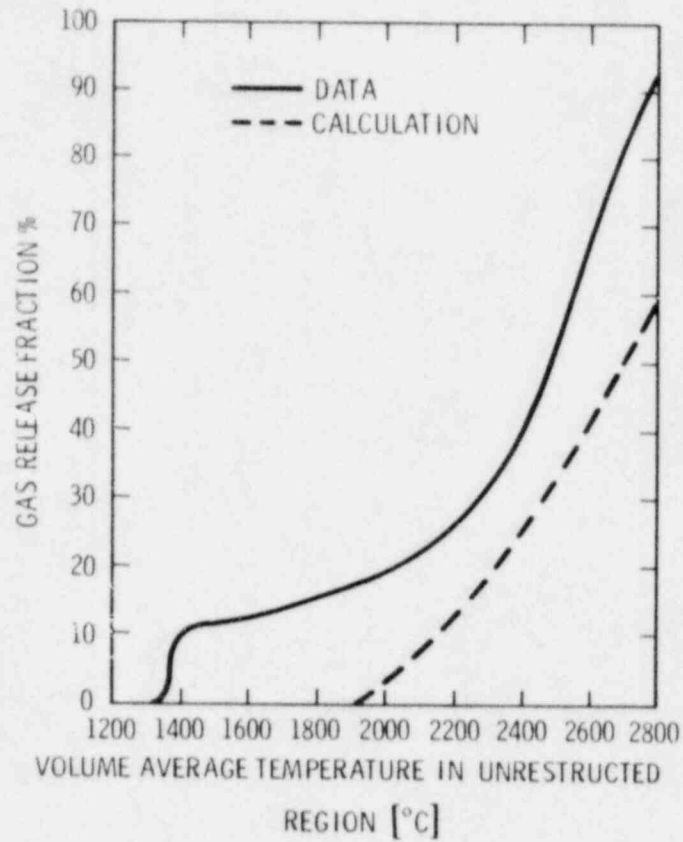
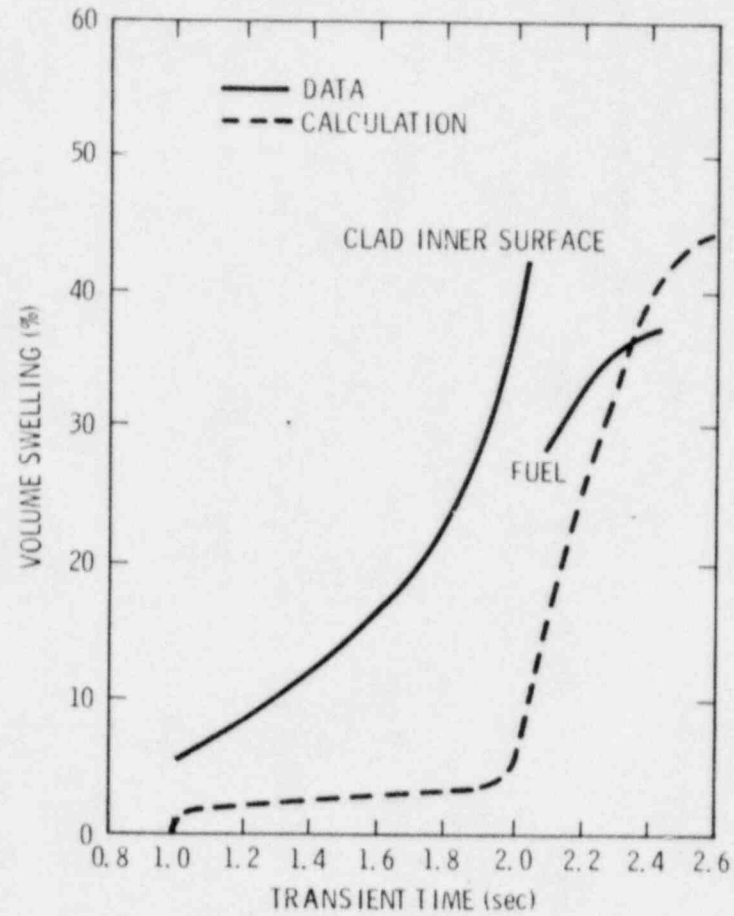FIGURE 2. CALCULATED GAS RELEASE COMPARED WITH FGR 39 DATA.

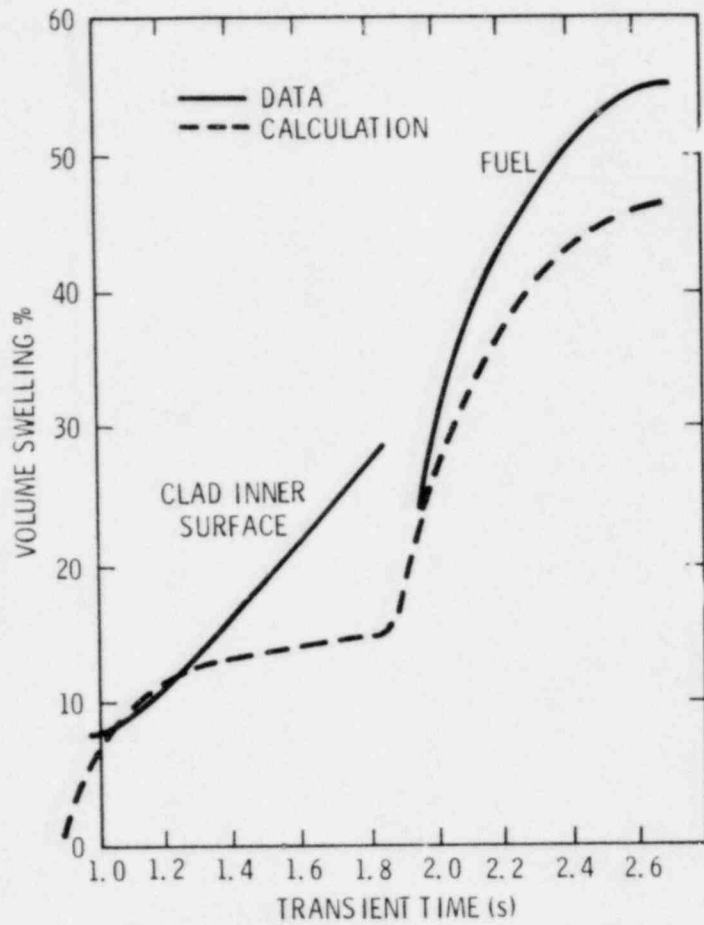FIGURE 3. CALCULATED SWELLING COMPARED WITH FD 1.4 DATA

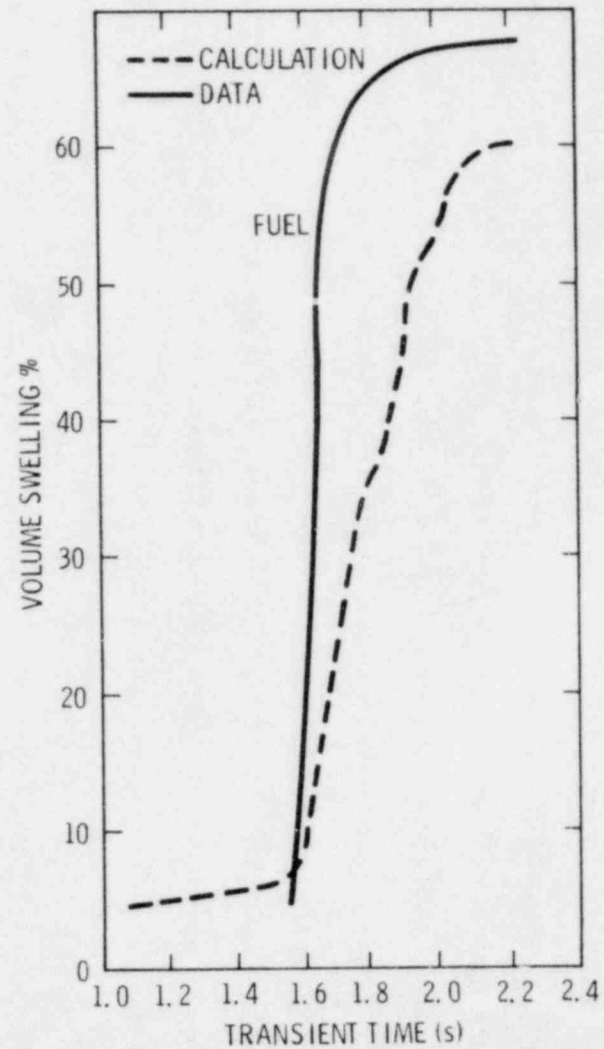FIGURE 4. CALCULATED SWELLING COMPARED
WITH FD 1.7 DATA.

FIGURE 5. CALCULATED SWELLING COMPARED WITH
FD 1.8 DATA.

rise in gas release which is about equal to the amount of gas on grain boundaries. A modification of the temperature distributions allowing for stoichiometric effects on thermal conductivity has been suggested[39] as a way to improve considerably the degree of agreement later in the transient.

The swelling data of experiments FD1.4, 1.7, and 1.8 are reproduced reasonably well provided the preexponential creep constant is increased a factor of ten from that tentatively suggested by the measurements of Slagle[25,41] on stoichiometric urania. The justification for treating the constant as a variable to be fitted depends on effects of grain size, density, fuel composition, and stoichiometry as discussed by Slagle, although theories of dislocation creep do not depend on grain size.[40] The effect of radial variations in stoichiometry[26] and fuel composition are likely to be very large and may even dominate radial variations in gas content. Also most of the swelling in the FD1 experiments occurred at temperatures close to or above the solidus (2998 K), whereas the highest temperatures in Slagle's measurements were about 100 K lower. The activation energy and power law exponent are as recommended by Slagle;[41]

$$\varepsilon = \kappa \, \sigma^{3.5} \, \exp\left(- \frac{1.5 \cdot 10^5}{T}\right). \tag{82}$$

Because of the difficulties indicated earlier in modeling large-scale swelling (grain distortion, creep geometry, creep rate, sensitivity to bubble overpressure and radius), the present modeling is not directed primarily at swelling calculations. Those calculations reported here should be seen only as demonstrating

the ability to produce swellings of roughly the correct order of magnitude at about the right time in the transients.

The agreement between calculation and data can be improved, but since the remaining discrepancies can be accounted for just as well by adjusting the details of the heating transient within experimental error as by changing parameters, it is felt that the underlying bubble dynamics are treated sufficiently well to enable meaningful results to be obtained on crack development. An observation worth noting is that in the results shown in Figures 2, 3, and 4 the greater part of the rapid swelling is by creep relaxation of intragranular bubbles with only about 5% volume swelling or less arising from grain face bubbles. The contribution from edge porosicy is not calculated. Including this may diminish the need to increase the creep constant.

5. OBSERVATIONS CONCERNING CRACK GROWTH

The results of the above calculations may be compared with the crack growth criteria of Section 2.

Figures 6, 7, and 8 show on a log scale the bubble pressure as a function of time in several radial nodes for experiments FGR39, FD1.7, and FD1.6. In FGR39,[7] fuel melt temperatures were achieved and fuel was lost from the test section. FD1.7 is taken to be typical of the FD1[4] experiments that exhibited rapid swelling without fuel dispersal and FD1.6 was an experiment[4,5] that produced very rapid fuel dispersal on a fine scale. The zones labeled in Figures 6 to 8 have the largest label towards the outer edge of the fuel pin.
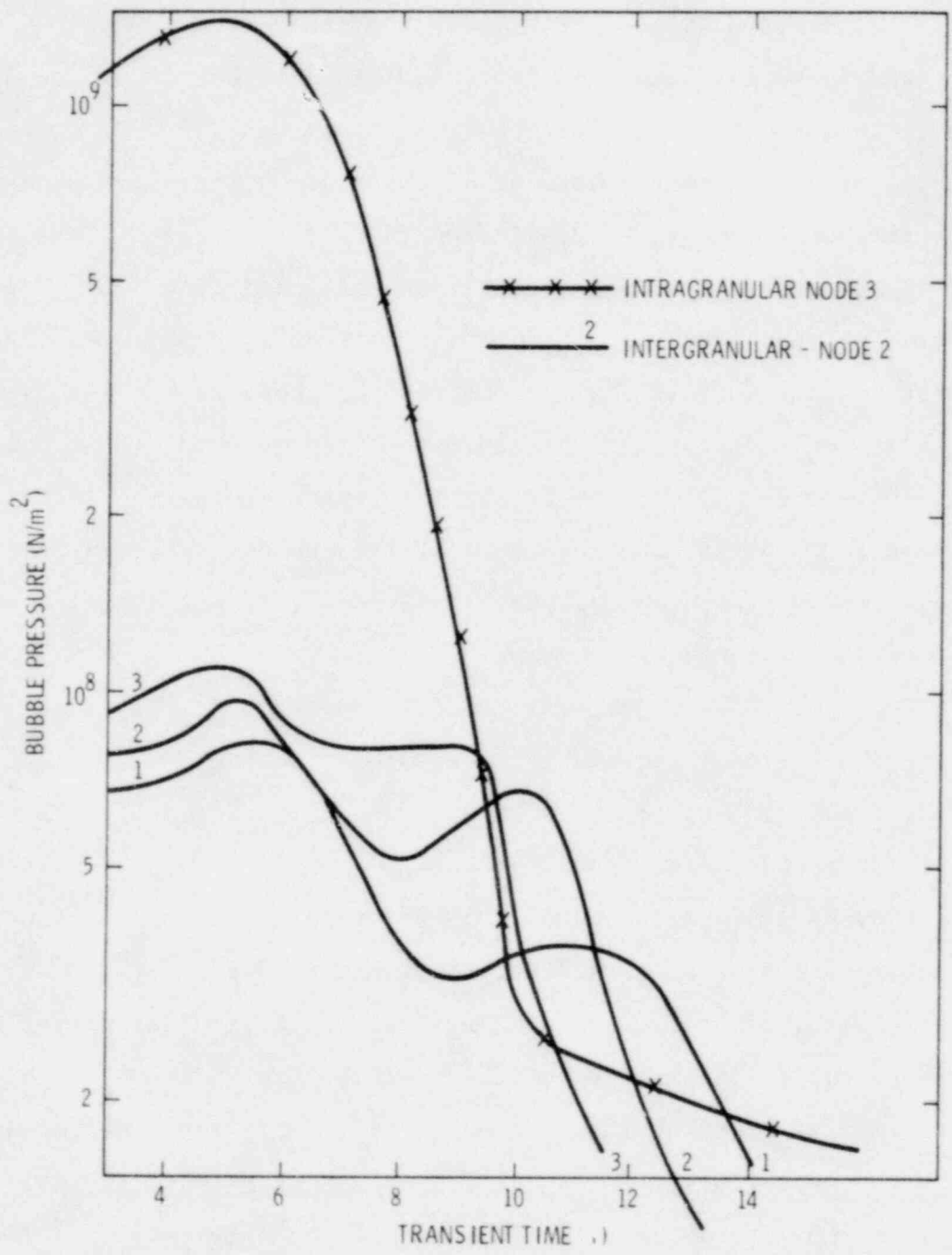
FIGURE 6. TOTAL INTERNAL BUBBLE PRESSURE CALCULATED FOR THE FGR 39 TRANSIENT.
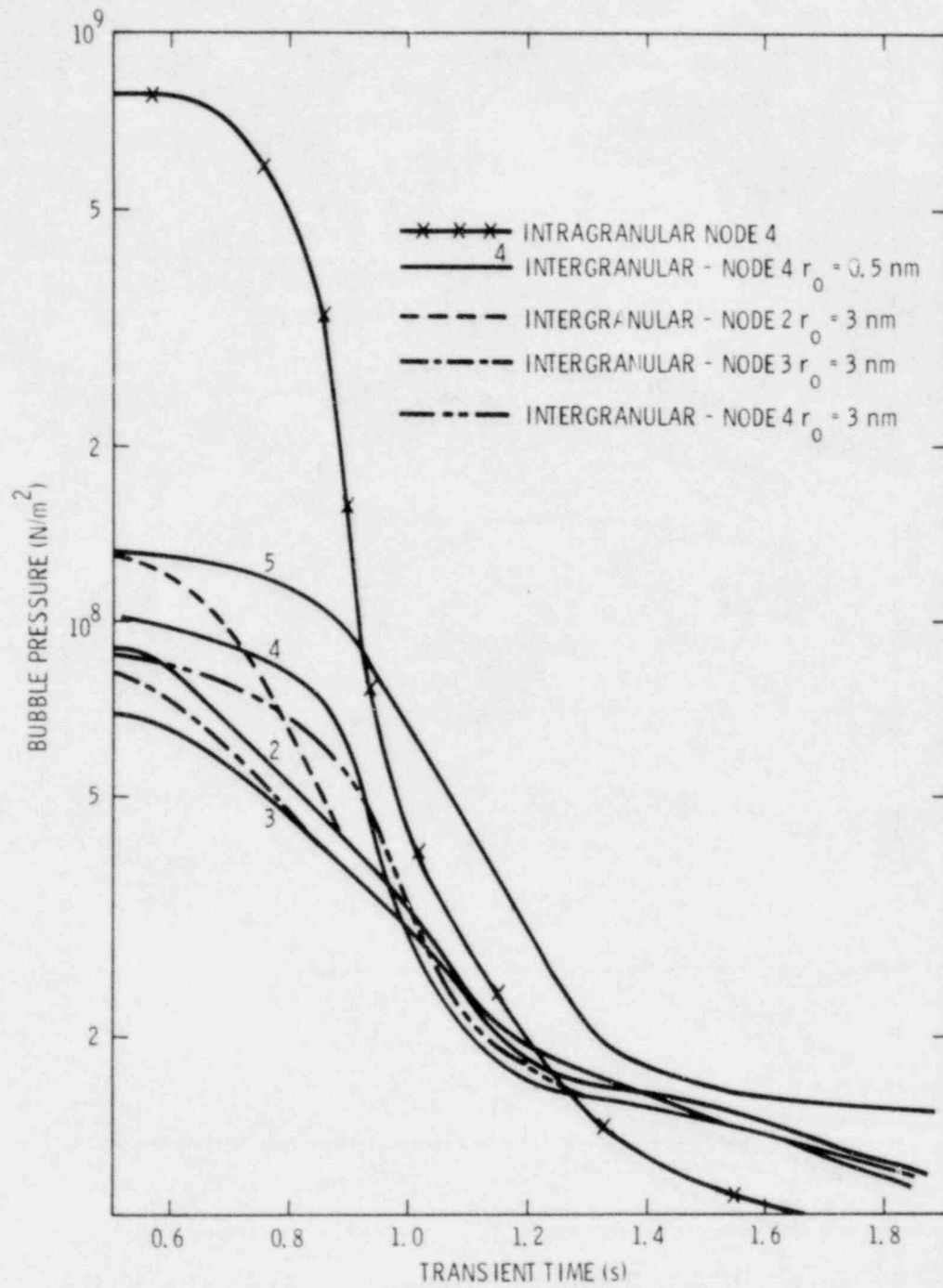
FIGURE 7. TOTAL INTERNAL BUBBLE PRESSURE CALCULATED FOR THE FD 1. 7 TRANSIENT.

The figure shows a plot of BUBBLE PRESSURE (N/m^2) on the vertical axis (ranging from below 10^8 to 10^9) versus TRANSIENT TIME (s) on the horizontal axis (from 0.6 to 1.8). The legend contains:

- ×—×—× INTRAGRANULAR NODE 4
- INTERGRANULAR - NODE 4 $r_0 = 0.5$ nm
- INTERGRANULAR - NODE 2 $r_0 = 3$ nm
- INTERGRANULAR - NODE 3 $r_0 = 3$ nm
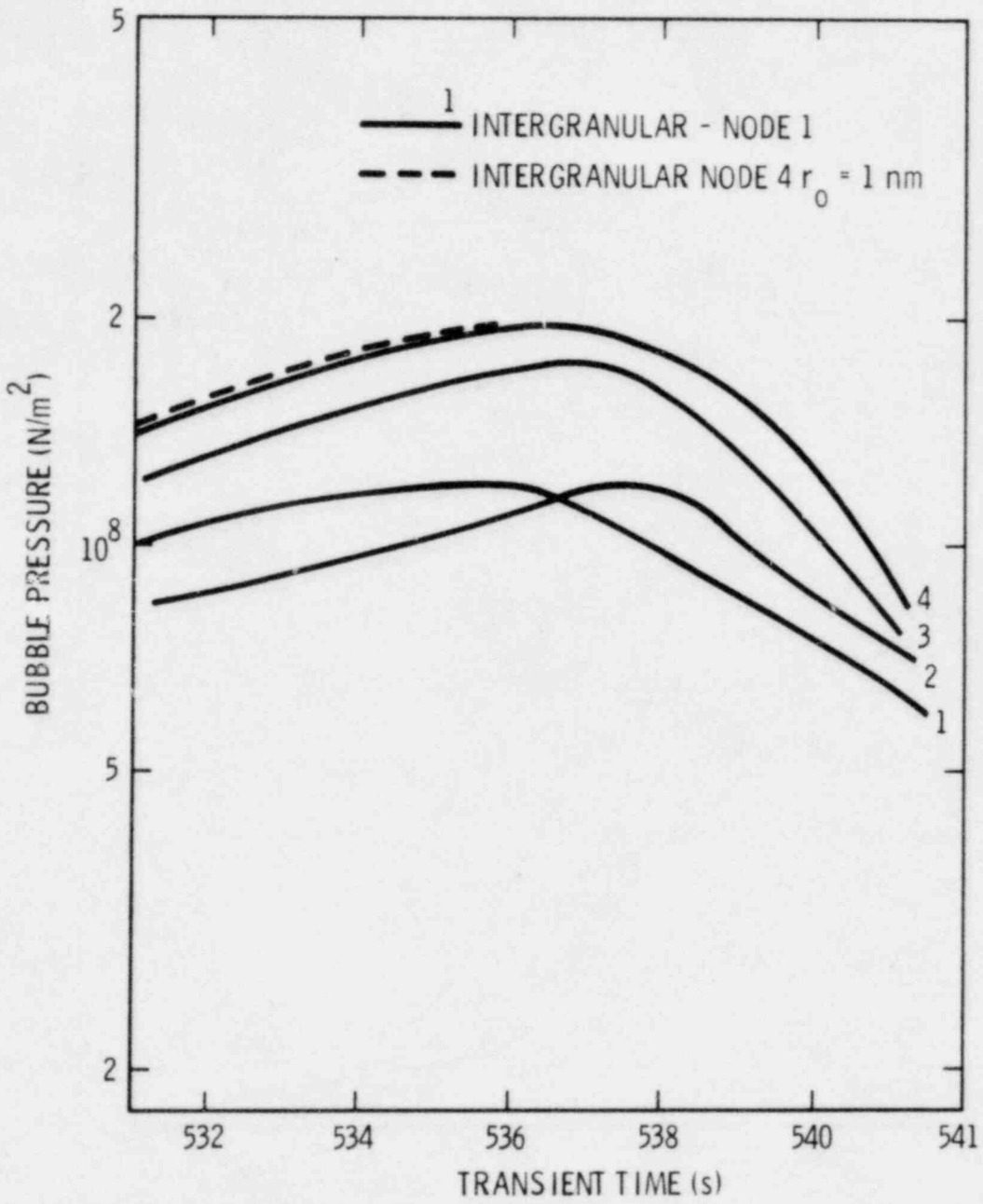- INTERGRANULAR - NODE 4 $r_0 = 3$ nm

FIGURE 8. TOTAL INTERNAL BUBBLE PRESSURE CALCULATED FOR
THE FD 1.6 TRANSIENT.

5.1 Stress Condition

Although the figures show only the total bubble pressure, the excess bubble pressures are generally an appreciable fraction of the total pressure. In FD1.7 and FGR39, at high temperatures excess bubble pressures reach the yield stress (~ 3 to 7×10^7 N/m^2) and considerably exceed it for FD1.6 ($\sim 10^8$ N/m^2) for intergranular bubbles. In all three transients the calculated excess intra-granular bubble pressures exceed the yield stress. Within the grains, therefore, a considerable proportion ($\sigma_r \propto \frac{1}{r^3}$) of the fuel matrix may be in a plastic state and on grain boundaries it seems likely that most of the interbubble region is plastic. However the excess bubble pressures are extremely sensitive to bubble size owing to the effect of both the Van der Waals equation-of-state for small bubbles and the subtraction of the surface tension term. For example, near the observed disruption time in FD1.6, a change of only +10% in intragranular bubble size produces a four-fold decrease in P_x. Under these circumstances to do more than note the possibility of plastic yielding is inappropriate and the subsequent analysis will ignore it.

At temperatures below 2000 K the brittle fracture stress is in the region of $1.0-1.5 \times 10^8$ N/m^2, and the stress criterion is only barely satisfied early in the transients even though bubble pressures are high for small bubbles.

5.2 Differential Energy Condition

5.2.1 Intergranular Bubbles

After early effects of initial conditions have damped out, bubble pressures are at least a factor of two higher in FD1.6

than in FGR39 or FD1.7. Moreover in FD1.6 the calculated pressures in all nodes exceed 10^8 N/m^2 which was earlier cautiously suggested as an appropriate criterion for crack advance. Note, also, that in nodes 1 to 4 the peak pressures occur around 537 ms, which was the time disruption was observed to commence. The effects of variations in the initial bubble size were considered. Figure 7 shows the result of increasing the initial intragranular bubble radius to 3 nm--a change in volume of two orders of magnitude. For such a large increase, nearly a whole second is required to reach a similar intergranular bubble configuration with the same pressures. Although not shown in the figure, the intragranular configuration converges rather more rapidly. For a tenfold increase in initial bubble volume (r_o = 1 nm) none of the nodes show a significant pressure change at 0.56 seconds.

In FD1.6 a tenfold increase in initial bubble volume also has little effect on the intergranular bubble pressures as the curve for node 4 shows.

Decreasing r_o to 0.3 nm (fivefold volume decrease) produces virtually no change from the standard case. Baker's measurements[38] showed nearly all the bubbles were of $r_o < 1$ nm. It may be concluded that the current pressure calculations are not very sensitive to the initial bubble size, providing this bubble size is ≤ 1 nm, and certainly after a few tenths of a second in the transient.

5.2.2 Intragranular Bubbles

In all three transients the intragranular bubble pressures are in the region of 3 to 15 x 10^8 N/m^2. This is probably enough to produce crack advance since whatever the criterion is for intergranular cracks ($1 \sim 2$ 10^8 N/m^2), using values of $2\gamma_s$ = 1.2 J/m^2 and $(2\gamma_s - \gamma_{gb})$ = 0.25 J/m^2, pressures need to be about a factor of five higher for the intragranular case. Since the surface energies are subject to considerable uncertainty, no definite conclusion is possible on this criterion. Bubble sizes and pressures calculated for different initial bubble sizes ($\leq$ 1 nm) converge closely after only about 0.3 seconds.

5.3 Total Energy Condition

Only intragranular cracks will be considered since grain boundary bubbles have reached a coverage fraction of 50% in all three transients by the time peak pressures are encountered and the discussion of Section 2.3 shows that the energy condition is then approximately satisfied.

The calculations show that the value of the ratio $E_{gas}/E_{surface}$ as defined in Section 2.3 maximizes in the range 0.01 to 0.4 for all nodes in all the transients. This indicates fairly clearly that intragranular bubbles are unlikely to be responsible for the disruption phenomena in FD1.6, as even the ratio values at the upper end of the above range do not take account of the random orientation of cracks. Note that this calculation depends on the bubble size and density as well as on the internal pressure.

5.4 Mass Transfer Condition

Figures 9 and 10 show the ratio between mass transfer rate tending to impart spheroidal shape and the bubble dynamics criterion (Eq. (48)) for FGR39 and FD1.6 for grain face bubbles. The labeled zones in Figures 9 and 10 have the largest label toward the outer edge of the fuel pin.

$$\text{Ratio} = \frac{\dot{V}_{sp}}{\left(\dfrac{V \dot{P}_g}{P_g} \right)} \; ; \; \dot{P}_g > 0 \; . \tag{83}$$

The ratio for FD1.7 is not relevant since apart from early transient effects (initial bubble size, discussed above) the pressures fall monotonically and are too low to induce crack growth. Although the pressures are not so low in FGR39, in the later periods of rising pressure the mass transfer rate is observed to be within an order of magnitude of being capable of arresting crack growth should it have occurred. Earlier in the transient the reverse is true and indications exist that loss of grain boundary adhesion could have taken place in all three radial nodes early in FGR39 had the pressure criterion been satisfied. The pressure in FGR39 is even less sensitive to initial conditions than the other transients because of the slowness of the heating. After a few seconds in FGR39, the pressure is near 10^8 N/m^2 and loss of grain boundary adhesion may have ensued. There appears to be no direct evidence that this did not occur to some extent since no posttest examination was performed, owing to subsequent fuel melting. An interesting observation is that the sudden gas

MASS TRANSFER RATIO

10^0

10^{-1}

10^{-2}

10^{-3}

10^{-4}

2   3   4   5   6   7   8   9   10   11   12   13

TRANSIENT TIME (s)

—— $\dot{P}_{BUBBLE\ DYNAMICS} > 0$
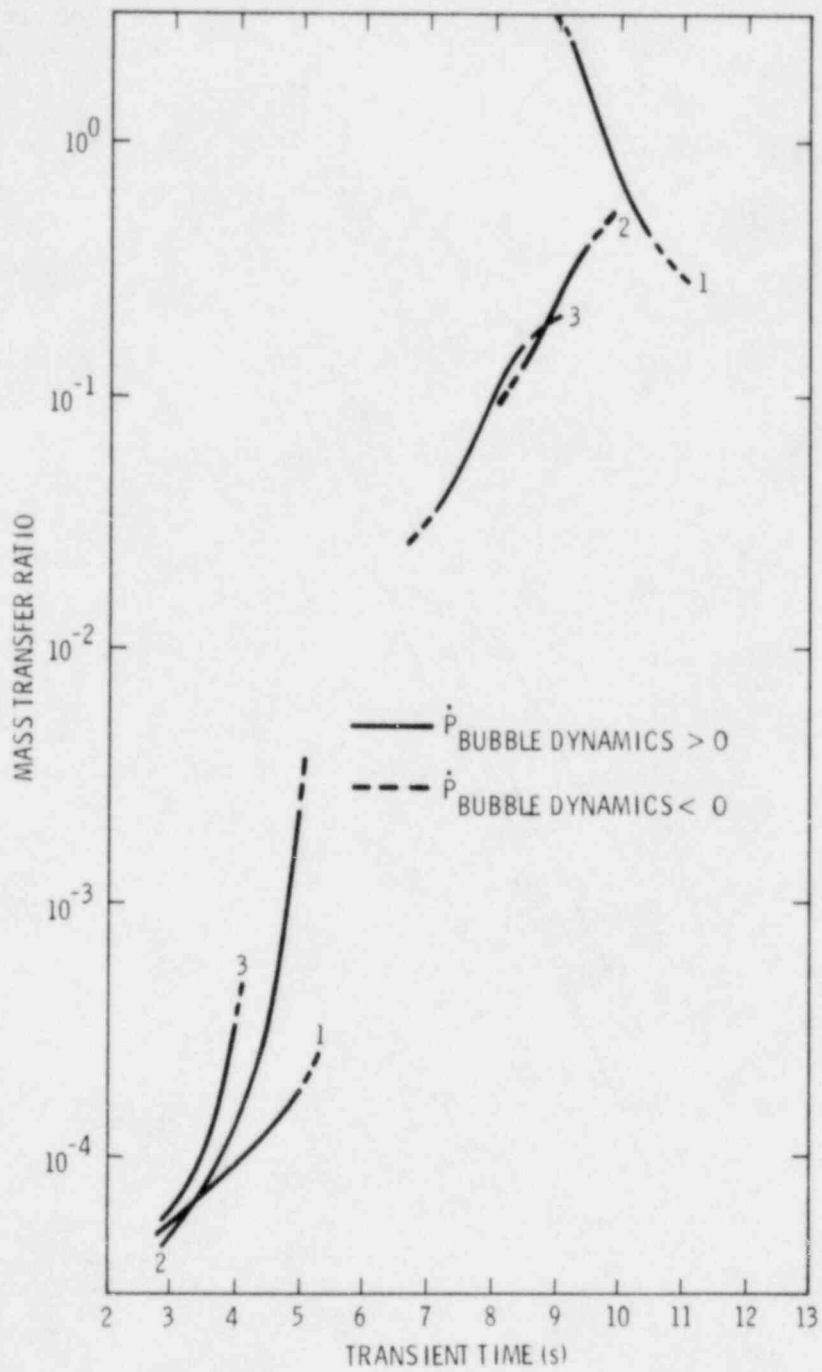
- - - $\dot{P}_{BUBBLE\ DYNAMICS} < 0$

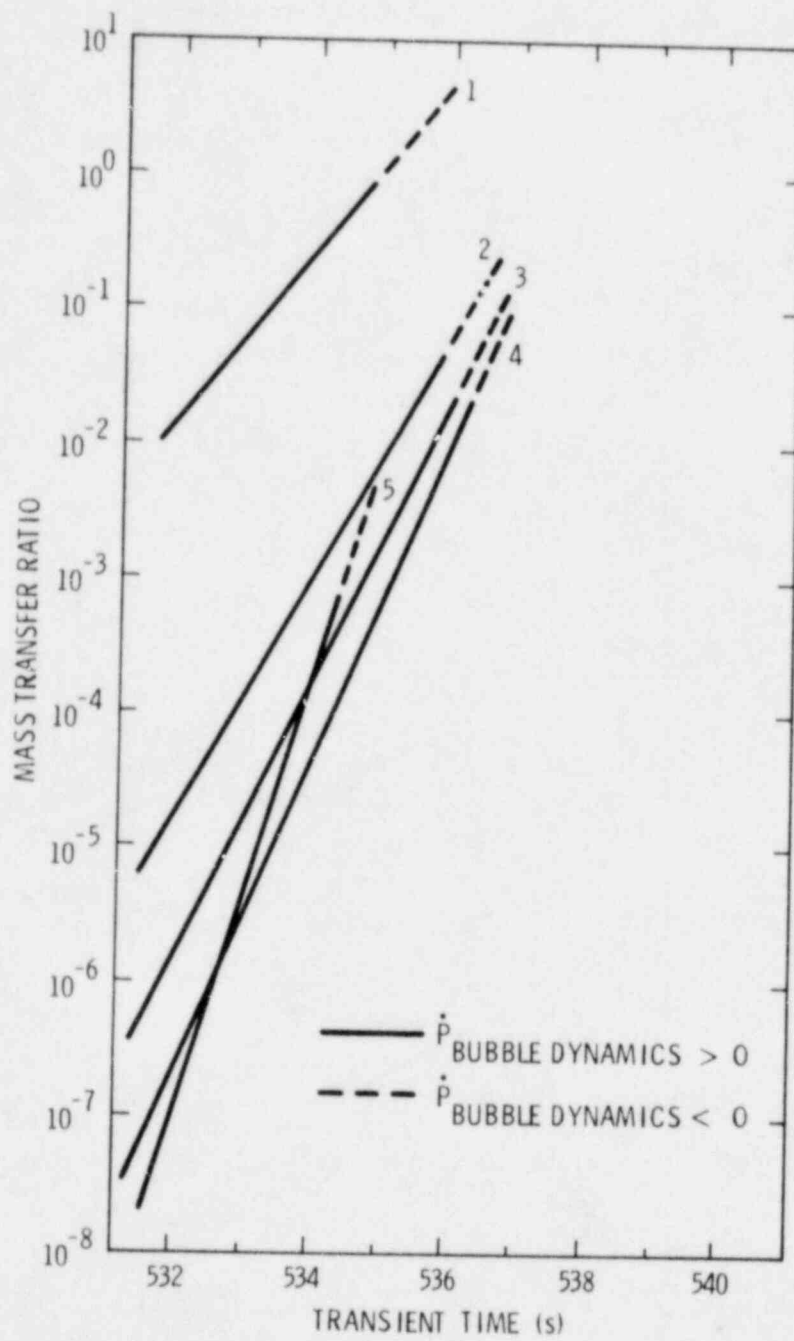FIGURE 9. MASS TRANSFER RATIOS CALCULATED FOR FGR 39.

53

FIGURE 10. MASS TRANSFER RATIOS CALCULATED FOR FD 1.6

release near the start of the transient suggests release of gas already present on grain boundaries. The author is not aware of any other explanation for this behavior.

A recent finding by Benson[44] that about 20% of retained fission gas can reside extragranularly in a fuel sample irradiated to 5.3% burnup at 26.3 kW/m lends some support to this hypothesis. On the other hand, the small radius of bubbles implied by temperatures below 1800 K early in transients suggests a higher critical pressure than 10^8 N/m^2 because a crack height of 2 nm is probably too large.

For FD1.6 the mass transfer ratio changes by eight orders of magnitude in about 6 ms during the second power pulse and approaches unity at about the observed dispersal time (537 to 538 ms) in only the innermost node. The mass transfer ratio is between one and two orders of magnitude too small in the other nodes at the observed dispersal time to prevent dispersal. This reinforces the indication from the experimental data[5] that disruption occurred below the fuel melting point which would not have been reached until 541 ms.

These calculations imply, therefore, that experiment FD1.6 attained the dispersal condition provided the pressure was high enough. This implies in turn that the critical pressure is somewhat larger than 10^8 N/m^2, or dispersal could have occurred any time after about 530 ms.

6. SUMMARY AND CONCLUSIONS

Internal bubble pressures have been noted to produce an important modification of the differential energy condition for crack advance. This modification stems from the large potential energy configuration derived from the stress system and renders details of the elastic/plastic strain configuration relatively unimportant. Such pressures are encountered during heating transients that produce rapid coalescence of bubbles in mechanical disequilibrium.

Appropriate mass transfer mechanisms are considered in the presence of cracks and related primarily to local curvature of internal surfaces in the fuel matrix. Mass transfer by surface diffusion along internal crack surfaces can arrest crack growth at high temperatures.

A very straightforward bubble dynamics calculation treating both intragranular and grain face bubbles has been used to examine conditions prevailing in typical examples of slow, fast, and very fast heating transients. This model was derived from aspects of the NEFIG,[27] FISGAS,[28] and FRAS[24] codes and was set up to account for phenomena that could influence grain boundary bubble pressures.

It has been found that intragranular bubble sizes and densities are not high enough to allow an interconnected network of intragranular cracks to develop although bubble pressures may attain the differential crack advance criterion. At high bubble densities on grain boundaries, all the criteria are sometimes achieved within the framework of the modeling. In applying the theory to experiment, it is important to realize that two

potentially large sources of uncertainty exist. One derives from the bubble dynamics calculation itself and the other from the numerical criteria used. Notwithstanding this difficulty the comparison with experiment reinforces the theoretical expectation that internal grain-face bubble pressures in the region of and somewhat larger than 10^8 N/m^2 are required to produce loss of grain-face adhesion.

In experiment FD1.7, the only time when conditions appear favorable to crack growth is near the start of the transient, at least before the second pulse. However, the bubble pressures fall off rather rapidly and monotonically and during the phase of rapid swelling are an order of magnitude too low to cause dispersal. In contrast, pressure peaks for FGR39 and FD1.6 occur at a later time. The calculated pressures are about a factor of two higher in FD1.6 than in FGR39. FD1.6 is the only experiment of the three that is known to have produced fine-scale fuel fragmentation.

A limited effort has been made to generalize the above conclusions by carrying out a number of calculations (about 20) on a variety of transients, for one fuel node characteristic of "gassy" fuel. The transients were all started from 1500 K and ranged over the following timescales:

a) Dwell times from 0.5 sec to 20 sec at temperatures from 1500 K to 2100 K, followed by heating ramps to 3000 K at rates varying from 1 K/msec to 300 K/msec.

b) Continuous linear heating ramps to 3000 K at rates from 0.1 K/msec to 300 K/msec.

Although the detailed results are too complex to discuss at
length, at the risk of introducing some oversimplification the
general trend of the results is as shown in Figure 11. These
results apply to grain boundary bubbles only.

Near the start of all the transients at temperatures below
2000 K, high pressures are developed early in small bubbles (r ~
few nanometers). These pressures result mainly from coalescence
within the grains. Although the overall pressures are high, the
criterion for crack advance in this range of bubble sizes is
probably higher than 10^8 N/m^2 because of small crack opening dis-
placements. Hatch marks in figure 11 are intended to display this
feature but should be interpreted as only an intuitive indication
below 2300 K. At such low temperatures the stress criterion may
be associated with the brittle fracture stress (~ 1.5×10^8 N/m^2)
rather than the value for yield stress adopted earlier for higher
temperatures (~ 5×10^7 N/m^2). Accounting for the stress concentra-
tion factor (Eq. (3)) suggests a stress criterion in the region
of $P_x \geq 5 \times 10^7$ N/m^2. Such excess pressures are not always convinc-
ingly exceeded for temperatures below 1800 K. A further, somewhat
stronger, argument for excluding this region from possible crack
propagation comes from the low bubble density on the grain boundary.
At this stage in the transients the bubbles do not possess enough
energy to propagate cracks to their neighbors.

According to the initial bubble size used, pressures at the
start can vary appreciably although after a few tenths of a second
these effects dissipate with pressures around 8×10^7 N/m^2. Heating
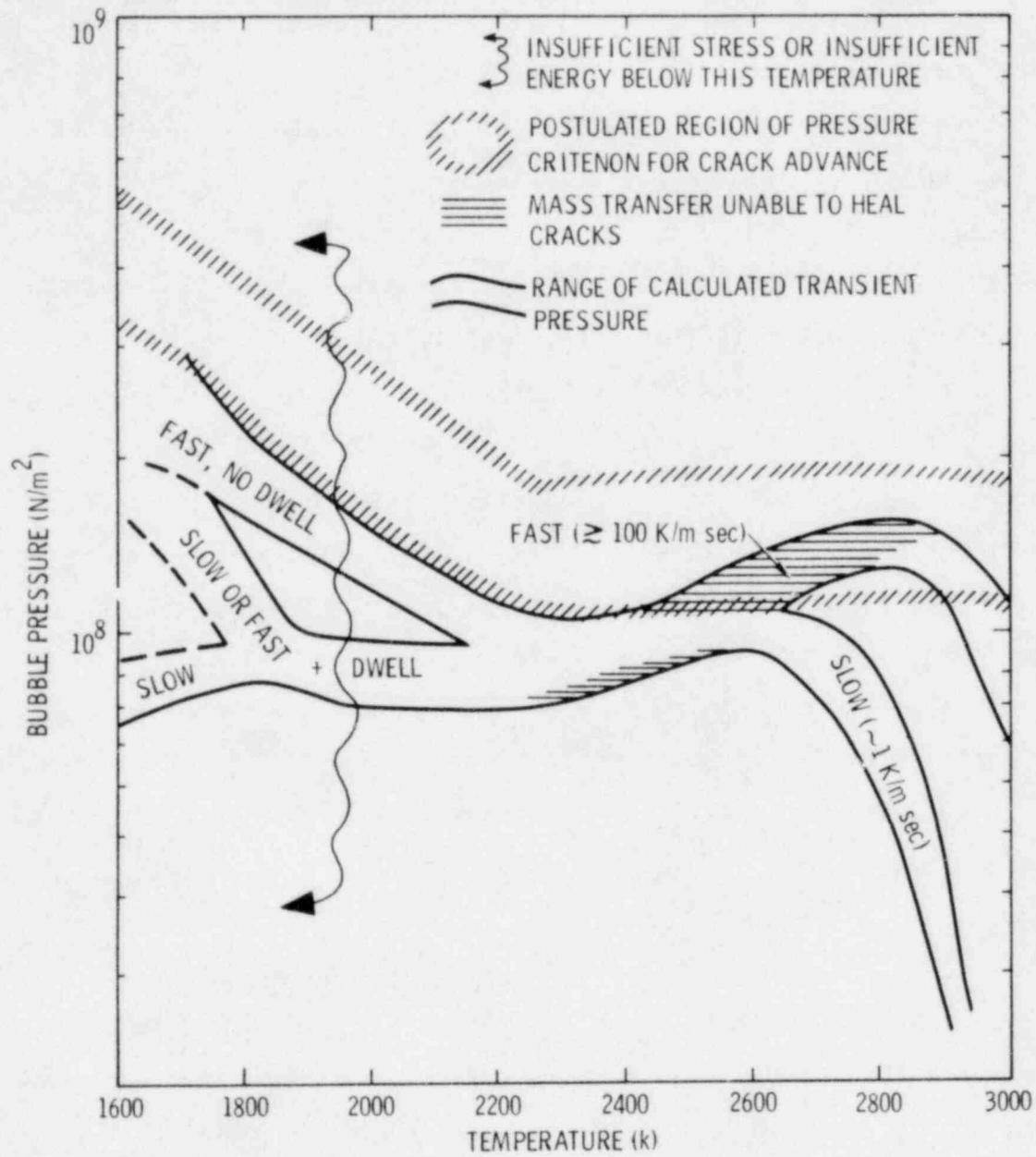through this low temperature region on a ms timescale leads to

FIGURE 11. GENERAL TREND OF CALCULATED BUBBLE PRESSURE FOR
RANGE OF TRANSIENTS.

higher pressures (factor of two or three) but these too fall to about 10^8 N/m^2 by 2400 K.

Because of the above effects, it seems unlikely that grain boundary separation could occur below 2000 K.

Above 2200 K the pressures rise until creep causes a reversal of slope below the melting point. The slower transients are much more susceptible than the fast ones to creep relaxation, and pressures barely reach 10^8 N/m^2. The faster transients rise to the postulated pressure criterion rather easily before creep intervenes within 100 K of the melting point.

Mass transfer at the cracks is thermally dominated and is generally able to heal cracks dynamically above about 2300 K for slow transients but not for the ms scale transients.

The consequence of these trends, although severely generalized, is that heating at rates of order 100 K/ms above 2300 K seems most likely to lead to fine-scale fuel disruption for a wide range of conditions earlier in the transient. Heating over a few seconds seems unlikely to achieve the same behavior. This is in accordance with the limited experimental evidence that exists.

Although the bubble pressures depend upon many features of the dynamics, some confidence in the calculated values may be derived from the observation that the gross high temperature swelling observed late in the FD1 experiments is approximately reproduced even though the principal mechanism appears to be intragranular bubble relaxation by creep which takes place at a rate proportional to P_x to the power 3.5. The model does not

give an appreciable contribution to the swelling from grain face bubbles since the amount of gas needed to saturate the available grain boundary is small. The contribution from edge porosity is not calculated.

Note that the present work is concerned only with the loss of internal structural stability that crack propagation implies. This is a necessary condition for fine scale dispersion but not a sufficient one. For FD1.6 the calculations were performed for the extreme axial end of the fuel column, in a system that required only 2 bars gauge pressure to allow fuel to escape from its confining end restraint. This is a low-constraint condition that would not be met in a reactor environment until clad failure or melt-off. The problem of investigating which types of transients are more likely to attain the crack growth criteria will be the subject of a separate study in conjunction with the Sandia Laboratories future experimental program. Only when these conditions are appreciated can they be associated with constraint conditions and real reactor accidents.

TABLE I

Parameter Values

B	Van der Waals constant	$8.5 \ 10^{-29} \ m^3$
λ	Surface diffusion boundary layer thickness	0.34 nm
Ω	Atomic volume	$4.1 \ 10^{-29} \ m^3$
Q_s^*	Heat of transport	0.42 MJ/mole
γ_s	Surface energy	$0.6 \ J/m^2$
$(2\gamma_s - \gamma_{gb})$	Modified surface energy	$0.25 \ J/m^2$

D_s	Surface diffusion coefficient	$3.5 \ \exp\left[-\dfrac{4.53 \ 10^4}{T}\right] m^2 s^{-1}$
D_g	Gas atom diffusion coefficient	$3.9 \ 10^{-6} \ \exp\left[-\dfrac{4.53 \ 10^4}{T}\right] m^2 s^{-1}$
D_u	Uranium ion self-diffusion coefficient	$2 \ 10^{-4} \ \exp\left[-\dfrac{5.56 \ 10^4}{T}\right] m^2 s^{-1}$
wD_{gb}	Grain boundary self-diffusion coefficient	$6.9 \ 10^{-16} \ \exp\left[-\dfrac{2.9 \ 10^4}{T}\right] m^2 s^{-1}$
$\dot{\varepsilon}$	Power law creep rate	$3.10^{-4} \ \sigma^{3.5} \ \exp\left[-\dfrac{1.5 \ 10^5}{T}\right] s^{-1}$

α	Coalescence parameter	1.0
g	Grain boundary strength parameter	0.1
$r(o)$	Initial bubble radius	0.5 nm
$n(o)$	Initial number of atoms per bubble	5.5

References

1. S. N. Hunter and D. H. Worledge, "A Cylindrical Model of Prompt Critical Excursions in a Fast Breeder Reactor," Private Communication, 1975.

2. L. W. Dietrich and J. F. Jackson, "Proceedings of the IWGFR Specialists' Meeting on the Role of Fission Products in Whole-Core Accidents," Harwell, July, 1977. IAEA Conf. Proceedings IWGFR/19.

3. G. Bandyopadhyay and J. A. Buzzell, "Role of Fission Gas and Fuel Melting in Fuel Response During Simulated Hypothetical Loss-of-Flow Transients," to be published in Nuclear Technology, (January, 1980).

4. G. L. Cano, R. W. Ostensen, M. F. Young, Visual Investigation of Reactor Fuels Response to Simulated LOF Heating Conditions, First Series, NUREG/CR-0914, SAND79-0940 R7, Sandia Laboratories, Albuquerque, NM, 1979.

5. D. H. Worledge and G. L. Cano, "Study of the Dispersive Potential of Irradiated Fuel Using In-Core Experiments," Proceedings of the ANS/ENS International Meeting on Fast Reactor Safety Technology, Seattle, WA, August, 1979.

6. C. Baker, "The Fission Gas Bubble Distribution in a Mixed-Oxide Fast Reactor Fuel Pin," J. Nucl. Mater., 75, 105, 1978.

7. C. A. Hinman and O. D. Slagle, Ex-Reactor Transient Fission Gas Release Studies--Fuel Pin PNL-2-4, HEDL TME 77-83, UC 79b, 1977.

8. R. E. Esteves, A. R. Wazzan and D. Okrent, "Elementary Model for Non-Equilibrium Fission Gas Behavior in a Fast Transient," Trans. Am. Nucl. Soc. 21, 180, 1975.

9. E. E. Gruber, W. R. Bohl and M. G. Stevenson, Analysis of Fuel Motion after Loss of Integrity of Pins, ANL-RDP-15, March, 1973.

10. P. T. Heald, An Introduction to Fracture Mechanics, CEGB, RD/B/N2844, 1973.

11. F. E. Bard and D. S. Dutt, HEDL-TME 72-28, 1972.

12. T. Yokobori, The Strength, Fracture and Fatigue of Metals, P. Nordhoff, Groningen, Netherlands, 1965, p. 145.

13. M. W. Finnis, AERE-R 8537, 1976.

References--cont'd

14. A. A. Griffith, Phil. Trans. Roy. Soc. (London) Ser. A. 221, 163, 1920.

15. R. Bullough and R. C. Perrin, "Growth, Stability and Inter-action of Voids and Gas Bubbles in Solids," Radiation Damage in Reactor Materials, Symposium Proceedings, Vienna 1969, Vol. 2, p. 233, STI/PUB/230.

16. J. F. Knott, Fundamentals of Fracture Mechanics, Wiley, 1973.

17. G. L. Reynolds and B. Burton, "Grain Boundary Diffusion and Uranium Dioxide: The Correlation between Sintering and Creep and a Reinterpretation of Creep Mechanism," J. Nucl. Mater. 82, 22, 1979.

18. C. E. Inglis, Trans. Instn. Nav. Archit. LV, 1, 219, 1913.

19. R. J. DiMelfi and L. W. Dietrich, "Modelling of the Effects of Grain Boundary Fission Gas on Transient Fuel Behavior," ANS Transactions 28, 237, 1978.

20. D. Hull and D. E. Rimmer, Phil. Mag. 4, 673, 1959.

21. M. V. Speight and J. E. Harris, Metal Sci. J. 1, 83, 1967.

22. D. R. Olander, Fundamental Aspects of Nuclear Reactor Fuel Elements, Ch. 18, TID-26711-P1, 1976.

23. J. M. Griesmeyer and N. M. Ghoniem, A Dynamic Intragranular Fission Gas Behavior Model, NUREG/CR-0906, 1979.

24. E. E. Gruber, "A Generalized Parametric Model for Transient Gas Release and Swelling in Oxide Fuels," Nucl. Tech. 35, 617, 1977.

25. O. D. Slagle, Deformation Behavior of UO_2 at Temperatures above 2400°C, HEDL-TME 78-31, UC 79b, 1978.

26. D. R. Olander, "Fundamental Aspects of Nuclear Reactor Fuel Elements," TID-26711-P1, 1976.

27. J. R. Matthews and M. H. Wood, "Modelling the Transient Behavior of Fission Gas," accepted for Publication in J. Nucl. Mater, 1979.

28. R. W. Ostensen, FISGAS--A Code for Fission Gas Migration and Fuel Swelling in an LMFBR Accident, SAND78-1790, Sandia Laboratories, Albuquerque, NM, 1979.

References--cont'd

29. G. W. Greenwood and M. V. Speight, J. Nucl. Mater. $\underline{10}$, 140, 1963.

30. S. Chandrasekhar, Rev. Mod. Phys. $\underline{15}$, 1, 1943.

31. P. G. Shewmon, Trans. Amer. Inst. Min. Metall. Pet. Eng. $\underline{230}$, 1134, 1964.

32. E. E. Gruber, J. Applied Phys. $\underline{38}$, 243, 1967.

33. Private Communication, W. J. Camp.

34. E. H. Randklev, "Radial Distribution of Retained Fission Gas in Irradiated Mixed-Oxide Fuel, Trans. Am. Nuc. Soc. $\underline{28}$, 234, 1978.

35. J. H. Scott, S. A. Chastain, T. T. Arey, E. D. Jenson, Preliminary Data Report, Post-Irradiation Examination of Fuel Pins, PNL-10-23 and PNL-10-63, HEDL TME 74-23, UC 79b, May, 1974.

36. G. L. Cano, to be published.

37. D. S. Dutt et al, Trans. Amer. Nucl. Soc. $\underline{15}$, 198, 1972.

38. C. Baker, "The Fission Gas Bubble Distribution in a Mixed Oxide Fast Reactor Fuel Pin," J. Nucl. Mater. $\underline{75}$, 105, 1978.

39. J. R. Matthews, Private Communication.

40. J. Gittus, Creep, Viscoelasticity and Creep Fracture in Solids, Applied Science Publishers, Ltd., London, 1975.

41. O. D. Slagle, Private Communication.

42. F. K. G. Odqvist, "Theory of Creep Under Combined Stresses with Application to High Temperature Machinery," Proc. Royal Swedish Academy of Eng. Research, $\underline{141}$, 31, 1936.

43. S. Timoshenko, Strength of Materials, Part II, p. 536, Van Nostrand, 1956.

44. D. A. Benson, private communication, 1979.

The Macroscopic Creep Rate for a Thick-Walled Sphere
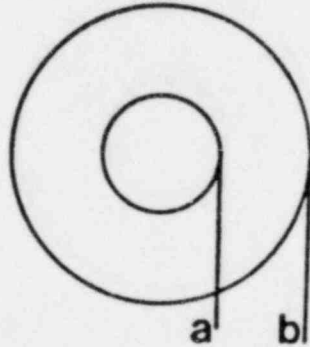
Fig. AI.1

Consider the above figure where a is the internal and b the external sphere radius.

Equilibrium in the thick wall requires that

$$\frac{r d\sigma_r}{dr} = 2(\sigma_t - \sigma_r) \qquad \text{AI.1}$$

where σ_r is the radial and σ_t the tangential stress component.

If u is the radial displacement, then the radial $(\varepsilon_r = \frac{du}{dr})$ and tangential $(\varepsilon_t = \frac{u}{r})$ strains can be combined to give:

$$\frac{d\varepsilon_t}{dr} = \frac{1}{r} (\varepsilon_r - \varepsilon_t). \qquad \text{AI.2}$$

The strain rates v_t and v_r, at least for short time intervals, are then related by

$$\frac{dv_t}{dr} = \frac{1}{r}(v_r - v_t). \qquad \text{AI.3}$$

The multiaxial strain rates depend on the effective stress σ_e in the way described by Odqvist.[42] Following the exposition of Timoshenko[43] they are related by

$$v_t = \frac{\kappa}{2} \sigma_e^{n-1} (\sigma_t - \sigma_r)$$

and

$$v_r = \kappa \sigma_e^{n-1} (\sigma_r - \sigma_t) \qquad\qquad \text{AI.4}$$

with

$$\sigma_e = \sigma_t - \sigma_r \qquad\qquad \text{AI.5}$$

and the uniaxial creep data represented by

$$v = \kappa \sigma^n \qquad \text{(see Eq. (60))} \qquad \text{AI.6}$$

Using Eqs. (AI.4) and (AI.5) to eliminate the v_i in Eq. (AI.3), the latter becomes:

$$\frac{d}{dr} (\sigma_t - \sigma_r)^n = - \frac{3}{r}(\sigma_t - \sigma_r)^n$$

from whence

$$(\sigma_t - \sigma_r)^n = \frac{c}{r^3} . \qquad\qquad \text{AI.7}$$

Substituting for $(\sigma_t - \sigma_r)$ from Eq. (AI.7) into Eq. (AI.1), gives a directly integrable equation for σ_r with two constants that can be determined from the boundary conditions,

$$\sigma_r(r = a) = -P_x \qquad\qquad \text{AI.8}$$

$$\sigma_r(r = b) = 0 \qquad \text{(for zero or negligible hydrostatic pressure)}.$$

σ_t is then determined from Eq. (AI.7).

The result gives for the radial creep rate

$$r \cdot v_t = \frac{\kappa}{2r^2} \left[\frac{3P_x}{2n\left(a^{-3/n} - b^{-3/n}\right)} \right]^n.$$ \qquad AI.9

This shows that the macroscopic creep term to be
added to Eq. (56) is given by

$$\dot{r}\bigg|_{r=a} = \frac{\kappa b^3}{2a^2} \left(\frac{3}{2n}\right)^n \left[\frac{P_x}{\left(\frac{b}{a}\right)^{3/n} - 1} \right]^n.$$ \qquad AI.10

APPENDIX II

Random and Biased Bubble Migration on the Grain Surface

1. Random Coalescence

The random coalescence rate is treated approximately as follows. Only the instantaneous rate is required and therefore the problem can be treated in a stationary approximation. Bubbles constantly arriving from the grain interior constitute a uniform source term over the boundary which maintains the bubble concentration approximately constant (ignoring effects of changing bubble size) at a distance x from the center of a bubble considered fixed in the grain boundary. The bubble concentration is a maximum at this point and falls to zero at the interaction distance $R = 2r_B$.

The diffusion equation is then

$$D_B \frac{1}{r} \frac{d}{dr}\left(\frac{rdc}{dr}\right) + S = 0. \qquad \text{AII.1}$$

The above boundary conditions are

$$C(R) = 0 \qquad \text{and} \qquad \frac{dc}{dr}\bigg|_x = 0. \qquad \text{AII.2}$$
$$C(x) = C_B$$

The solution is the same type as used in Eq. (32) and gives

$$-D_B \frac{dC}{dr}\bigg|_R = \frac{-D_b \, C_B}{R} \left[\frac{(1 - R^2/x^2)}{\ln\left(\frac{x}{R}\right) - \frac{1}{2}\left(\frac{x^2 - R^2}{x^2}\right)} \right]. \qquad \text{AII.3}$$

The term in square brackets takes values in the range 0.5 to 1.5 as the coverage fraction varies from 0.1 to 0.7 and is approximated by a constant value of unity.

The number of coalescence events per unit volume is then given by multiplying the flux of Eq. (AII.3) by the area of height R and radius R, which surrounds the capture volume, and the bubble concentration.

$$\dot{C}_B = -D_B \, C_B^2 \, \frac{2\pi R}{R} \cdot R \, . \qquad \qquad \text{AII.4}$$

Since there are N bubbles on a grain area given by:
(see Section 3.2)

$$A = 0.67 \times \frac{1}{2} \times 4\pi \left(\frac{d}{2}\right)^2 , \qquad \qquad \text{AII.5}$$

$$C_B = \frac{N}{0.67 \, \pi d^2 \, r_B} \, . \qquad \qquad \text{AII.6}$$

Consequently Eq. (AII.4) can be written as

$$\dot{N}\Bigg|_{\text{random}} = -\frac{4 \, D_B \, N^2}{0.67 \, d^2} \, . \qquad \qquad \text{AII.7}$$

However the problem has been solved using a stationary original bubble, and a factor of two must be included in D_B to correct for the case of moving bubbles.[30] Furthermore the bubble diffusion coefficient as given by Olander[20] for surface diffusion

should be multiplied by $\frac{3}{2}$ to account for the necessary modification of the Einstein equation in two dimensions,

$$D_B = \frac{9}{4} \frac{\lambda^4 D_s}{\pi r_B^4} \times 2 . \qquad \text{AII.8}$$

Consequently for random coalescence alone

$$\dot{N}\Big|_{\text{random}} = - \frac{N^2 \ 18 \ \lambda^4 \ D_s}{0.67 \ d^2 \ \pi \ r_B^4} . \qquad \text{AII.9}$$

2. Biased Motion Coalescence

Each bubble sweeps out an interaction area $(2r_B)^2 v_B$ per unit time. Consequently

$$\dot{C}_B\Big|_{\text{biased}} = -4 \ r_B^2 \ v_B \ C_B^2 . \qquad \text{AII.10}$$

Using Eq. (AII.6), this becomes

$$\dot{N}\Big|_{\text{biased}} = \frac{4}{0.67 \ \pi} \frac{N^2}{d^2} r_B v_B \qquad \text{AII.11}$$

In applying Eqs. (AII.9) and (AII.11) to Eq. (72), the total coalescence rate among bubbles already on the grain boundary is

$$\dot{N}_2 = \dot{N}/_{\text{random}} + \dot{N}/_{\text{biased}} \qquad \text{AII.12}$$

with the coalescence parameter included in $\dot{N}/_{\text{biased}}$.

DISTRIBUTION:

U. S. Nuclear Regulatory Commission
(360 copies for R7)
Division of Document Control
Distribution Services Branch
7920 Norfolk Avenue
Bethesda, MD   20014

U. S. Nuclear Regulatory Commission (4)
Division of Reactor Safety Research
Office of Nuclear Regulatory Research
Washington, DC   20555
Attn: C. N. Kelber, Assistant Director,
            Advanced Reactor Safety Research
        R. T. Curtis, Chief
            Analytical Advanced Reactor Safety Research, ARSR
        M. Silberberg, Chief
            Experimental Fast Reactor Safety
        R. W. Wright
            Experimental Fast Reactor Safety

U. S. Department of Energy
Office of Nuclear Safety Coordination
Washington, DC   20545
Attn: R. W. Barber

U. S. Department of Energy (2)
Albuquerque Operations Office
P. O. Box 5400
Albuquerque, NM   87185
Attn: J. R. Roeder, Director
            Operational Safety Division
        D. K. Nowl: ., Director
            Special Programs Division
            For: C. B. Quinn
                   D. Plymale

W. E. Nyer
P. O. Box 1845
Idaho Falls, ID   83401

Projekt Schneller Brueter (4)
Kernforschungszentrum Karlsruhe GMBH
Postfach 3640
D75 Karlsruhe
West Germany
Attn: Dr. Kessler (2)
        Dr. Heusener (2)

Distribution (cont'd)

Institut de Protection
  et de Surete Nucleaire (3)
CEN Fontenay-aux-Roses
B. P. 6
France
Attn: M. Tanguy
       M. Schmitt
       M. Cogne

Safety Studies Laboratory (3)
Commissariat a L'Energie Atomique
Centre d'Etudes Nucleaires de Cadarache
B. P. 1, 13115 Saint-Paul-les-Durance
Bouches-du-Rhone
France
Attn: M. Bailly
       M. Meyer Heine
       M. Penet

Centre d'Etudes Nucleaires de Grenoble
B. P. 85 - Centre de Tri
38401 Genoble, Cedex
France
Attn: M. Costa

UKAEA (18)
Safety and Reliability Directorate
Wigshaw Lane
Culcheth
Warrington, WA3 4NE
England
Attn: H. J. Teague (3)
       D. H. Worledge (15)

R. G. Bellamy
Reactor Fuels Group
AERE Harwell
Oxfordshire, OX11 ORA
England

R. G. Tyror, Head
REactor Development Division
UKAEA - Atomic Energy Establishment
Winfrith, Dorchester
Dorset
England

Joint Research Centre (2)
Ispra Establishment
21020 Ispra (Varese)
Italy
Attn: R. Klersy
       H. Holtbecker

Distribution (cont'd)

Power Reactor & Nuclear Fuel (3)
  Development Corporation (PNC)
Fast Breeder Reactor Development Project (FBR)
9-13, 1-Chome, Akasaka
Minato-Ku, Tokyo, Japan
Attn: Dr. Mochizuki
       Dr. Watanabe (2)

1100	C. D. Broyles	
1550	F. W. Neilson	
	Attn:	O. J. Burchett, 1552
		J. H. Gieske, 1552
2150	T. L. Workman	
4000	A. Narath	
4230	J. E. Powell	
4400	A. W. Snyder	
4410	D. J. McCloskey	
4420	J. V. Walker (5)	
4421	R. L. Coats	
4422	D. A. Powers	
4422	J. B. Rivard	
4422	D. W. Varela	
4423	P. S. Pickard	
4423	G. L. Cano	
4423	D. A. McArthur	
4423	A. C. Marshall	
4423	K. O. Reil	
4424	M. J. Clauser	
4424	D. C. Williams	
4425	W. J. Camp	
4425	W. M. Breitung	
4425	R. J. Lipinski	
4425	M. L. Schwarz	
4425	F. Briscoe	
4425	M. F. Young	
4426	G. F. Derbenwick	
4426	K. T. Stalker	
4426	S. A. Wright	
4442	W. A. Von Riesemann	
4450	J. A. Reuscher	
5500	O. E. Jones	
5530	W. Herrmann	
5800	R. S. Claassen	
5820	R. E. Whan	
5830	M. J. Davis	
5840	N. J. Magnani	
5846	R. A. Sallach	
5846	E. K. Beauchamp	
8266	E. A. Aas	
3141	T. L. Werner (5)	
3151	W. L. Garner (3)	
	For:	DOE/TIC (Unlimited Release)
3154-3	R. P. Campbell (25)	
	For:	NRC Distribution to NTIS